Received: 19 June 2020 | Revised: 25 September 2020 | Accepted: 30 October 2020

DOI: 10.1002/suco.202000345

Check for updates

fib CEB-FIP WILEY

TECHNICAL PAPER

Blind competition on the numerical simulation of steel-fiber-reinforced concrete beams failing in shear

Joaquim Barros[1] | Beatriz Sanz[2] | Petr Kabele[3] | Rena C. Yu[4] | Günther Meschke[5] | Jaime Planas[6] | Vitor Cunha[7] | Antonio Caggiano[8] | Nilüfer Ozyurt[9] | Ventura Gouveia[10] | Ab van den Bos[11] | Elisa Poveda[4] | Erez Gal[12] | Jan Cervenka[13] | Gerrit E. Neu[5] | Pierre Rossi[14] | Daniel Dias-da-Costa[15] | Peter K. Juhasz[16] | David Cendon[2] | Gonzalo Ruiz[4] | Tiago Valente[17]

[1]Full Professor, Department of Civil Engineering, School of Engineering, University of Minho, Guimarães, Portugal

[2]Associate Professor, Department of Materials Science, Technical University of Madrid, ETS de Ingenieros de Caminos, Madrid, Spain

[3]Department of Mechanics, Czech Technical University in Prague, Prague, Czech Republic

[4]Departamento de Mecánica Aplicada e Ingeniería de Proyectos, University of Castilla-La Mancha, Ciudad Real, Spain

[5]Department for Civil and Environmental Engineering Sciences, Ruhr University Bochum, Bochum, Germany

[6]Department of Materials Science, Technical University of Madrid, Madrid, Spain

[7]ISISE, Institute of Science and Innovation for Bio-Sustainability (IB-S), Department of Civil Engineering, University of Minho, Braga, Portugal

[8]Institut für Werkstoffe im Bauwesen, Technische Universität Darmstadt, Darmstadt, Germany

[9]Department of Civil Engineering, Bogazici University, Istanbul, Turkey

[10]Department of Civil Engineering, Polytechnic Institute of Viseu, Viseu, Portugal

[11]DIANAFEA, Delft, Netherlands

[12]Department of Structural Engineering, Ben-Gurion University of Negev, Be'er Sheva, Israel

[13]Červenka Consulting s.r.o, Prague, Czech Republic

[14]Institut Français des Sciences et Technologies des Transports, de l'Aménagement et des Réseaux, University of Eiffel, Paris, France

[15]School of Civil Engineering, The University of Sydney, Sydney, Australia

[16]Department of Mechanics, Materials and Structures, Budapest University of Technology and Economics, Budapest, Hungary

[17]Structural Design and Software Development, CiviTest-Pesquisa de Novos Materiais para a Engenharia Civil, Vila Nova de Famalicao, Portugal

Correspondence
Joaquim Barros, Institute for Sustainability and Innovation in Structural Engineering (ISISE), Department of Civil Engineering, School of Engineering, University of Minho, Campus de Azurém, 4800-058 Guimarães, Portugal.
Email: barros@civil.uminho.pt

Funding information
PGC2018-097116-A-I00, Grant/Award Number: MCIU/AEI/FEDER UE; Portuguese Science Foundation (FCT),

Abstract

Experimental research has shown the extraordinary potential of the addition of short fibers to cement-based materials by improving significantly the behavior of concrete structures for serviceability and ultimate limit states. Software based on the finite element method has been used for the simulation of the material nonlinear behavior of fiber-reinforced concrete (FRC) structures. The applicability of the existing approaches has often been assessed by simulating experimental tests with structural elements, in general of a small scale, where the parameter values of the material constitutive laws are adjusted for the aimed predicting level, which constitutes an inverse technique of arguable

Discussion on this paper must be submitted within two months of the print publication. The discussion will then be published in print, along with the authors' closure, if any, approximately nine months after the print publication.

 © 2020 *fib*. International Federation for Structural Concrete

Grant/Award Number: ICoSyTec Project reference PTDC/ECI-CON/27990/201

utility for structural design practice. For assessing the predictive performance of these approaches, a blind simulation competition was organized. Two twin T-cross section steel FRC beams, flexurally reinforced with steel bars and without conventional shear reinforcement in the critical shear span, were experimentally tested up to failure. Despite the experimental data provided for the definition of the relevant model parameters, inaccuracies on the load capacity, deflection, and strain at peak load attained 40, 113, and 600%, respectively. Inadequate failure modes and highly different results were estimated with the same commercial software, indicating the need for deeper analysis and understanding of the models and influence of their parameters on their predictive performance.

KEYWORDS

benchmark, fiber-reinforced concrete, material nonlinear finite element analysis, reinforced concrete beams, shear failure

1 | INTRODUCTION

The introduction entails three subsections: the first shows the potentialities of fiber reinforcement for concrete structural applications; the second provides a short description of the type of models based on the finite element method (FEM) for the analysis and design of fiber-reinforced concrete (FRC) structures; and the third contextualizes the performed blind simulation competition (BSC) and its objectives.

1.1 | Fiber reinforcement for concrete structural applications

Experimental research and emblematic constructions show the extraordinary potential of short fibers for the reinforcement of cement-based materials by improving the behavior of concrete structures significantly (whether they include conventional reinforcements or not) for serviceability limit state (SLS) and ultimate limit state (ULS) design conditions.[1–6] Regarding SLS, the smaller crack width and stress level in conventional reinforcements and higher stiffness of FRC structures in the post-cracking stage should be highlighted. In terms of ULS, the higher load-carrying capacity, more ductile failure modes, larger energy absorption and dissipation capacity, and better structural integrity under loading conditions representative of extreme events are of note.[3–5] In this paper, when a FRC structure includes conventional reinforcement the acronym R/FRC is used. The shear resisting mechanisms in FRC involve fiber pullout and aggregate interlock in mutual interdependency, since the resistance to the crack opening offered by fibers that bridge the crack faces increases the crack shear stress transfer capacity due to aggregate interlock effect.[7,8] Due to the presence of the aggregates in the shear crack, relative sliding of the faces is followed by their opening,[9] which pulls the fibers. The direction of the fiber pullout force, however, changes in this sliding-opening process,[10] which exhibits a magnitude that depends on the distribution and geometry of aggregates and fiber distribution and orientation. Due to the favorable synergetic effect of fiber pullout and aggregate interlock shear resisting mechanisms, fiber reinforcement has been intensively explored for eliminating totally, or partially, the conventional transverse reinforcement.[11–18]

Fiber reinforcement also provides significant enhancements in the durability and life cycle of concrete structures.[19,20] The main applications of FRC remain in flooring,[21–23] tunnelling[2–6,24] and in prefabrication,[25] though they are scarce in the development of innovative structural systems where the benefits of fiber-reinforcement mechanisms have a recognized potential for obtaining technical and economic advantages regarding conventional systems.[1,26,27]

Fibers, when crossed by cracks, develop reinforcement mechanisms through their pullout resistance, whose effectiveness depends on their material and geometric properties, on the mechanical properties of the surrounding cement paste, and on the fiber distribution and orientation in the element to build. The last ones are dependent on the technology of FRC application, its rheological properties, and geometry of the element to be produced.[28–31]

1.2 | Numerical approaches for modeling the behavior of FRC structures

The technical and economic benefits from fiber reinforcement may be mobilized for the development of innovative and sustainable FRC structural systems. However,

due to the aforementioned complex phenomena, design should be executed by using computational models of high sophistication at the level of computational mechanics and at the approaches that simulate the behavior of the constituent materials from the fresh[32] up to the hardened stage of the FRC.[33] Commercial software (C_S) based on the finite element method (FEM) has been used for the simulation of the nonlinear material behavior of FRC structures, as the contribution of fiber reinforcement is mainly activated after the fibers have been crossed by cracks. Smeared crack and discrete crack models (SCM and DCM, respectively) are the most implemented approaches.[34–43] However, the applicability of such approaches has been assessed by simulating experimental tests with elements, in general, of a small scale, where the values of their parameters are adjusted for the aimed predicting level, which constitutes an inverse technique of arguable utility for structural design practice. The majority of these models consider the contribution of fiber-reinforcement mechanisms through a cohesive traction-separation law obtained from semiempirical recommendations, or from experimental results, either directly or from inverse analysis (IA).[44] However, there is still considerable uncertainty regarding the most adequate methodology to derive the values of the model parameters for analyzing a given structure. An inadequate assessment of these values provides results without any representativeness of the real behavior of the structure. Designers are aware of this, which justifies the relatively low use of computational tools for exploring the advantages of FRC on the development of competitive and sustainable R/FRC solutions.

The fracture mode I parameters of the constitutive models of the most used FEM-based software for the analysis of R/FRC structures are obtained by executing an IA and using the experimental data determined in three-point notched beam-bending tests (3PNBBT) and in round panel tests (RPT). The IA with the 3PNBBT is recommended for 1D-type R/FRC structures for obtaining a stress versus crack width relationship (σ-w) capable of reflecting the wall effect of the element mold

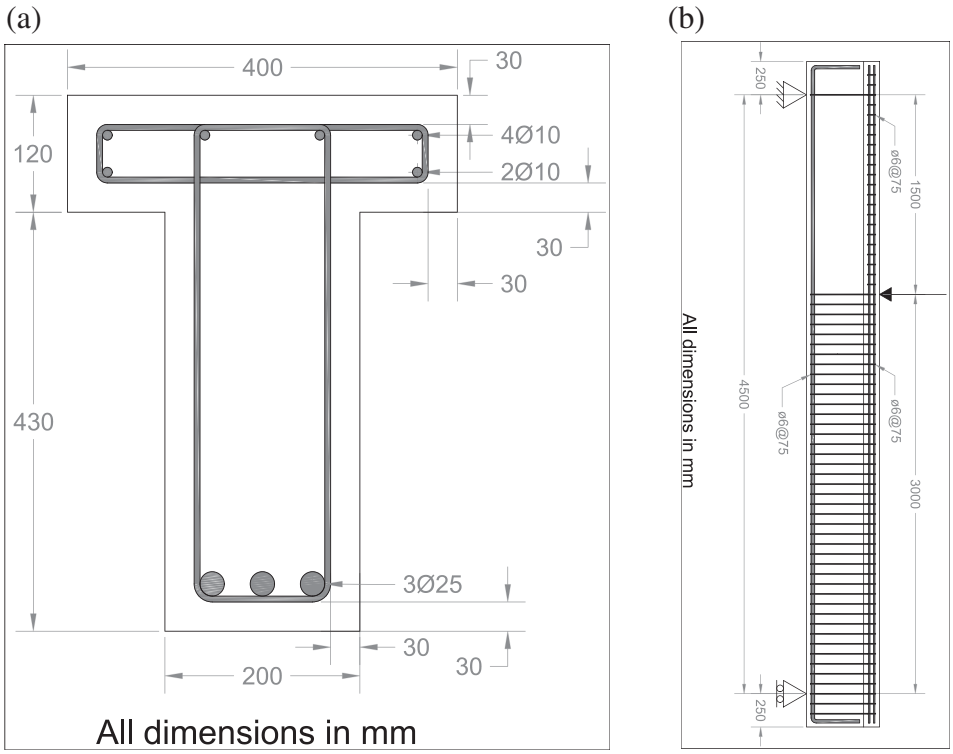


FIGURE 1 Geometry of the beam: (a) cross section and (b) longitudinal view (dimensions in mm)

TABLE 1 Composition of the SFRC

Aggregates (kg/m³)					Additives (kg/m³)			
CA	FA	CS	FS	CEM (kg/m³)	P	SP	w/c ratio (–)	Cf (kg/m³)
631	145	622	306	450	4.5	5.4	0.4	60

Abbreviations: CA, coarse aggregate 6/14; CEM, cement; Cf, Content of fibers; CS, coarse sand; FA, fine aggregate 4/8; FS, fine sand; P, plasticizer; SP, superplasticizer; w/c, water to cement ratio.

TABLE 2 Properties of the SFRC at seven and 14 days of age: average compressive strength (f_{cm}) and secant modulus of elasticity in compression (E_{cm}), limit of proportionality ($f_{f,Lm}$), and residual flexural strengths (f_{Rim}, i = 1–4) (STD values in MPa)

		Age (days)	
	Property	**7**	**14**
Compression	f_{cm} (MPa)	56.9 (0.7)	64.2 (1.5)
	E_{cm} (GPa)	30.3 (0.7)	32.9 (0.4)
Bending	$f_{f,Lm}$ (MPa)	5.63 (0.29)	5.57 (0.16)
	$f_{R,1m}$ (MPa)	4.76 (0.94)	4.79 (0.70)
	$f_{R,2m}$ (MPa)	4.67 (0.84)	4.21 (0.56)
	$f_{R,3m}$ (MPa)	3.49 (0.74)	3.16 (0.52)
	$f_{R,4m}$ (MPa)	2.80 (0.57)	2.49 (0.41)

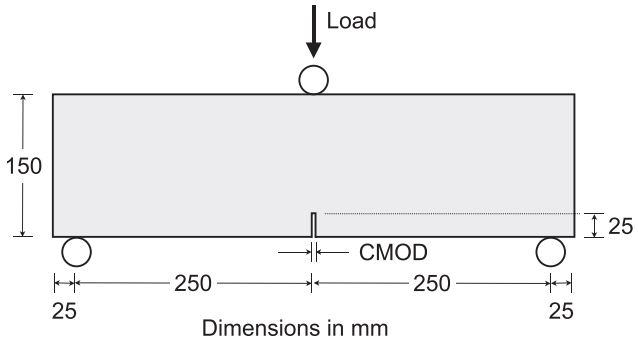


FIGURE 2 Localisation of the crack mouth opening displacement (CMOD) in the three-point notched beam-bending tests

and rheological properties of the FRC on the fiber orientation and distribution. For deriving the σ-w in the case of slabs and shell type R/FRC structures, IA applied to the results obtained in RPT is recommended, since in this test the fiber distribution and orientation, as well as the higher number of cracks of different orientation, regarding the 3PNBBT, best reflect the cracking process on these type of R/FRC structures.[45] However, available information in this respect shows that the σ-w relationships derived from the IA provide unsafe predictions.[46]

Another important aspect on the simulation of FRC structures entails consideration of the dispersion of results in the 3PNBBT and RPT in the constitutive laws simulating the FRC. Due to the relatively smaller fracture surface of these specimens regarding the total fracture surface occurred in real R/FRC structures, mainly in those of high-statically indeterminacy, the number of fibers that contributes to the post-cracking tensile capacity is smaller than in real structures, which results in a higher coefficient of variation values in these small-scale tests.

In the context of SCM, crack shear stress transfer is generally simulated by using a shear retention factor that can be a constant value,[47] or function of entities related to the opening/sliding process of the crack, including maximum aggregate size,[48,49] and reinforcement in the cracking zone.[50] Alternatively, a crack shear softening diagram has also been used.[51,52] However, the evaluation of the values for the parameters that define this diagram still requires reliable experimental test methodologies and design recommendations.

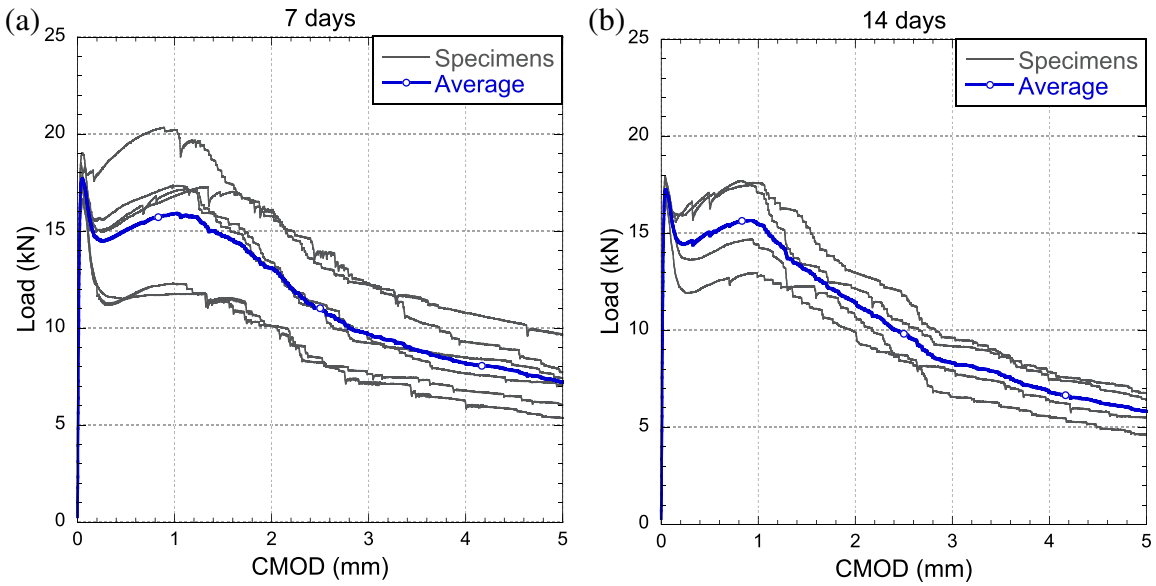


FIGURE 3 Load versus crack mouth opening displacement (CMOD) relationships in the three-point notched beam-bending tests executed at (a) 7 days and (b) 14 days

1.3 | BSCs and objectives of the present work

As shown in the previous sections, several analytical and numerical models have been developed over the past decades to reproduce the behavior of FRC. However, it is necessary a thorough understanding of their limitations in order to avoid unrealistic results. Moreover, the need for reducing the potential errors in modeling, analysis, and interpretation of results was pointed out by Vecchio.[53] As an example, the results corresponding to an international competition that involves reinforced concrete panels showed that predicted ultimate strength and strains were much higher than the experimental values.[54] Thus, BSC provide an opportunity to compare the results obtained by different methods and identify potentialities and weaknesses of the models.

Recently, some databases with R/FRC beams failing in shear have been proposed[55–57] with the objective of being a useful and reliable tool for assessing the predictive performance of analytical formulations and design

TABLE 3 Yield stress and tensile strength of the used three diameter steel bars (STD values in MPa)

Rebar diameter (mm)	Yield stress (MPa)	Tensile strength (MPa)
6	527 (11)	700 (16)
10	538 (7)	696 (6)
25	557 (2)	678 (1)

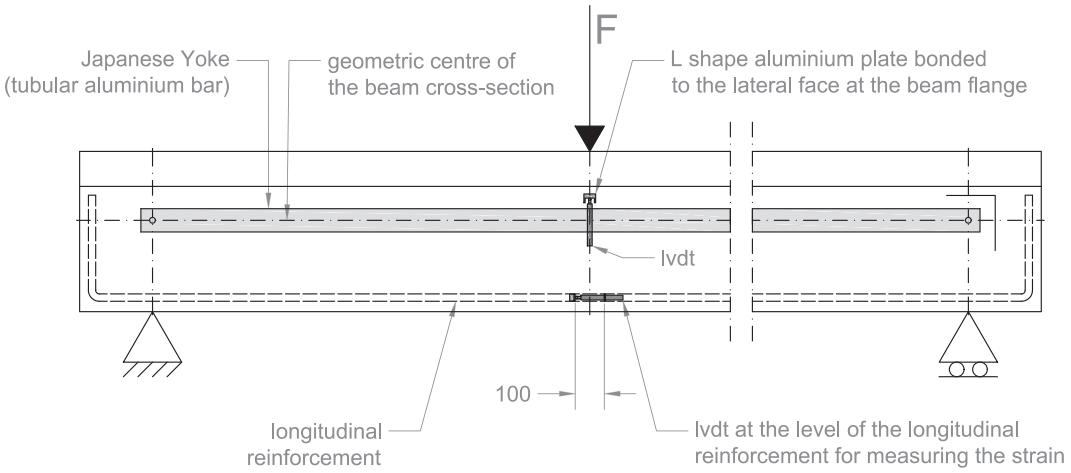


FIGURE 4 Sketch of the measurements of deflection and strain of the beam (dimensions in mm). LVDT, displacement transducer

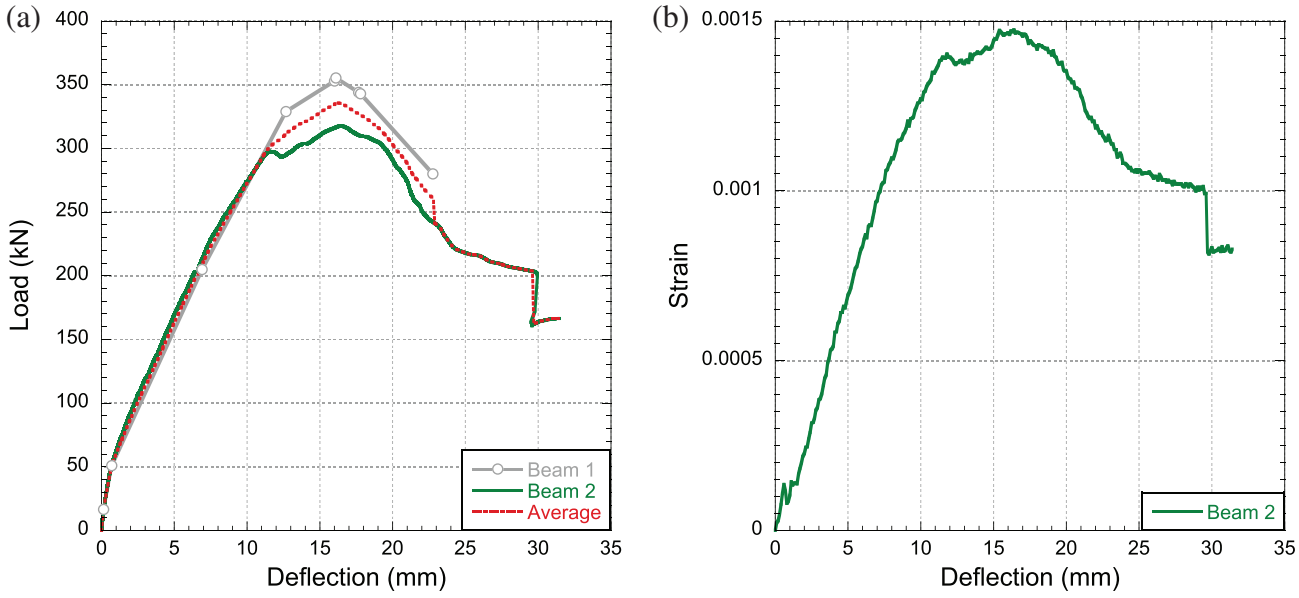


FIGURE 5 Experimental results: (a) average curves of load versus deflection and (b) and strain versus deflection

guidelines. However, these databases, in general, do not include fundamental information for the assessment of the predictive performance of more sophisticated models, namely those based on the FEM that are becoming more popular in design practice. For assessing the predictive performance of this type of models, other information like the deformational response, crack pattern and strain and stress fields in the constituent materials should be available. This is the main reason behind the BSC promoted by the *fib* Working Group WG 2.4.1-Modeling of FRC structures. This BSC sought to contribute to the assessment of the reliability of existing FEM-based approaches on the prediction of the relevant behavioral features of R/SFRC beams failing in shear. The present paper offers a description of this BSC, including the experimental program, the evaluation and classification processes, and provides a first preliminary set of observations based on the obtained information. It is not the intention to provide a deep discussion on the potentialities and weaknesses of the models used by the participants, since this will need the straight collaboration of some of the candidates, by performing extra simulations for extracting reliable conclusions of useful applicability in the design practice using the corresponding models.

2 | RULES OF THE COMPETITION AND INFORMATION PROVIDED TO THE PARTICIPANTS

2.1 | Rules of the competition

The BSC was announced at the end of 2019. The rules included information about the objective, geometry of the specimens, materials, test procedure, report to be prepared by the participants, criteria for selecting the best prediction and deadlines for the submission of the proposal.

The main objective was to obtain information about the performance of the models typically used to simulate the behavior of FRC structures. For that purpose, the response of a T-beam subjected to a three-point loading configuration up to failure was analyzed. The curves of load versus deflection and concrete strain (at the level of the longitudinal reinforcement) versus deflection, measured at the loaded section, were compared with those obtained from experiments.

The specimen consisted of a T-cross section steel FRC beam with conventional longitudinal (R/SFRC) and without conventional shear reinforcement in the critical shear span, as shown in Section 2.2.1.

The material properties of the SFRC were determined at 7 and 14 days by using standardized tests.[58] The values of these properties are indicated in Section 2.2.2 and were available to the participants in the last week of January and first week of February 2020.

The test procedure involved subjecting two twin beams to eccentric loading under displacement control until failure. Details can be found in Section 3.1. The participants were required to reproduce the experiment by using numerical models and provide the load-deflection and strain-deflection obtained from the numerical simulations.

The proposals in conditions to be accepted were sent prior to 23.59 (central-European time, CET) on February 29, 2020, to the secretariat of the *fib* WG 2.4.1. The reports from participants had to include the following:

a. A document limited to four pages with a given format, where a description of the fundamental aspects of the model used in the simulation was suggested.

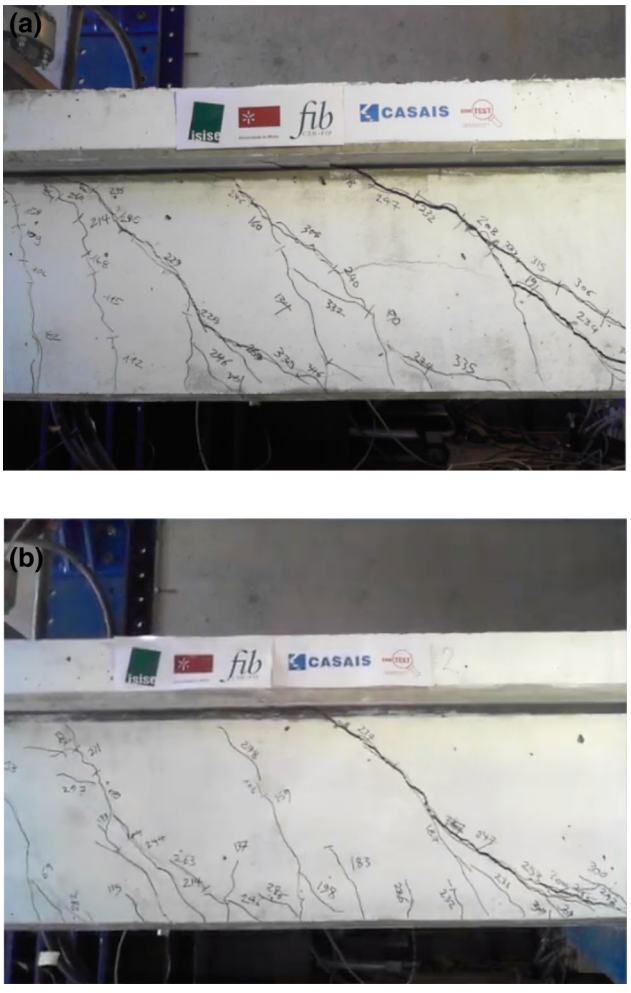


FIGURE 6 Crack pattern at failure of beam in the short shear span region: (a) 1 and (b) 2

TABLE 4 Predictive performance of the numerical simulations presented by the participants (shown in random order)

Participant no.	Rel. error of F_{max} $\Delta F/F$ (%)	ERR force–deflection Err_F (%)	Rel. error of strain at F_{max} $\frac{\Delta\varepsilon}{\varepsilon}$ (%)	ERR strain-deflection Err_ε (%)	Rel. error of deflect. at F_{max} $\Delta u/u$ (%)	Score (%)	Ranking	Class of model	Type of software
1	16.12	59.71	22.70	86.05	47.83	36.05	6	SCM	C_S
2	14.34	62.43	18.60	83.45	49.69	34.83	5	SCM	IH_S
3	18.09	34.06	84.04	77.77	16.15	42.65	10	CDP	C_S
4	51.88	44.91	2,486	60.18	356.5	705.8	32	CDP	C_S
5	4.417	9.356	201.8	260.9	3.106	79.96	21	CDP	C_S
6	7.973	89.26	12.45	122.3	69.57	41.96	9	SCM	IH_S
7	41.93	27.09	1824	78.23	136.0	503.0	31	SCM	C_S
8	32.99	77.10	41.78	54.37	18.63	41.79	8	Others	IH_S
9	42.55	89.62	86.10	102.7	38.51	65.90	17	SCM	C_S
10	1.270	6.135	33.56	23.50	4.348	12.76	1	SCM	IH_S
11	83.12	122.0	129.9	59.78	57.76	94.52	24	CDP	C_S
12a	53.73	35.02	1,562	70.48	223.0	455.1	29	CDP	C_S
12b	34.85	32.26	182.9	80.08	0.000	70.76	19	SCM	C_S
13	60.80	29.14	1.659e + 5	2.020e + 4	241.0	4.355e + 4	36	SCM	C_S
14	70.55	23.65	2,376	136.3	831.7	760.7	34	DCM	IH_S
15	8.847	53.34	28.99	64.63	23.60	28.35	2	SCM	IH_S
16	13.48	42.25	43.63	57.98	24.84	31.49	3	CDP	C_S
17	42.22	46.37	92.66	75.46	147.8	74.62	20	CDP	C_S
18	11.68	21.01	109.7	66.46	23.60	44.86	11	LDPM	IH_S
19	42.66	22.38	112.1	29.47	40.37	55.31	14	Others	IH_S
20	32.98	29.90	226.9	87.49	6.211	82.44	22	SCM	C_S
21	9.844	27.78	95.48	138.6	18.01	48.04	13	DCM	IH_S
22	28.74	105.5	89.36	90.55	78.88	69.11	18	CDP	C_S
23	49.19	52.64	93.35	64.81	20.50	58.01	15	SCM	C_S
24	30.44	14.41	332.8	64.10	24.84	106.2	26	SCM	C_S
25	66.59	45.88	56.46	59.22	72.05	61.03	16	CDP	C_S
26	30.34	48.69	49.33	43.07	23.60	38.10	7	SCM	C_S
27	46.45	38.31	1,199	86.52	86.34	343.5	27	SCM	C_S
28	35.35	31.33	1,464	121.5	30.43	399.7	28	SCM	C_S

(Continues)

TABLE 4 (Continued)

Participant no.	Rel. error of F_{max} $\Delta F/F$ (%)	ERR force–deflection Err_F (%)	Rel. error of strain at F_{max} $\frac{\Delta\varepsilon}{\varepsilon}$ (%)	ERR strain-deflection Err_ε (%)	Rel. error of deflect. at F_{max} $\Delta u/u$ (%)	Score (%)	Ranking	Class of model	Type of software
29	53.46	58.72	167.1	135.8	9.317	84.27	23	CDP	C_S
30	41.35	16.64	4,040	834.3	167.1	1,135	35	SCM	IH_S
31	78.28	30.08	2,498	517.3	215.5	740.5	33	Others	IH_S
32	39.16	24.89	90.62	54.91	10.56	47.17	12	DCM	IH_S
33	13.12	7.442	81.23	54.63	3.106	31.95	4	SCM	IH_S
34	42.87	27.05	1.955e+9	1.622e+8	346.6	5.049e+8	37	Others	IH_S
35	147.5	168.4	966.5	32.34	983.9	469.3	30	CDP	C_S
36	98.55	99.73	97.34	104.9	99.38	99.18	25	LDPM	IH_S

Abbreviations: CDP, concrete damage plasticity; C_S, commercial software; DCM, discrete crack models; LDPM, lattice discrete particle models; IH_S, in-house software; SCM, smeared crack models.

b. A spreadsheet in .xls format with the results of the simulations, which contained three columns: one for the deflection, one for the load, and one for the strain, obtained every 0.1 mm of deflection.
c. An image file (in jpeg or pdf format) of the crack pattern obtained at peak load.

After the participant predictions were received, two twin R/SFRC beams were tested up to failure under a three-point loading configuration, in order to obtain the experimental response and to compare it with the results of the numerical simulations. The experimental tests were carried out in the laboratory of the Structural Division of the Department of Civil Engineering of Minho University (LEST), on March 9, 2020, coinciding with the 10th meeting of the *fib* WG 2.4.1. The experiments were live-streamed through a YouTube Channel (first test: https://youtu.be/lWssVtSx3eI, second test: https://youtu.be/8AM5ehch0EA).

For the selection of the best simulation in reproducing the experimental results, the force-deflection and strain-deflection response were considered, together with the capacity to predict the maximum load, and the strain and deflection corresponding to that. The criterion to calculate the performance level of a simulation is detailed in Section 4.1. The quality of the crack pattern prediction was planned to be considered only in case of tied participants.

The conclusions about the processing of results were sent to the participants in mid-April 2020. A report that contained the main results and an additional file with the experimental records of deflection, load, and strain were sent to the participants. For the comparison of results and for a preliminary analysis of the obtained simulations, see Section 4 and Section 5.

2.2 | Information provided to the participants

2.2.1 | Geometry of the beams, support and loading conditions

Figure 1 shows a sketch of the geometry of the specimen, support and loading conditions. The specimen consists of a T-cross section beam reinforced with longitudinal bars in the bottom of the web and in the flange. Shear stirrups were disposed in the largest shear span, in the full length of the flange, and in the zone of the supports, as represented in the figure. A concrete cover thickness of 30 mm was adopted. Three-point bending was applied with an eccentric load, thus dividing the specimen in two shear spans with different length.

2.2.2 | Mix composition of the SFRC and properties

The mix design was coordinated by the company CiviTest (www.civitest.com). The SFRC was supplied by Unibetão at the request of Casais company (www.casais.pt) that produced the two twin beams. The composition of the SFRC is indicated in Table 1, corresponding to a concrete C50/60 XD3 (P) CL 0.20 D_{max} 12.5 S5, with a type cement CEM II/A-L 42.5R of fast hardening of 58.8 and 67.1 MPa at seven and 28 days, respectively.

Hooked end steel fibers of 33 mm length, 0.55 mm diameter, and tensile strength higher than 1,100 MPa were used (information provided by the supplier of the fibers). The density of the SFRC at 7 and 14 days was, respectively, 2,376 and 2,400 kg/m^3. The compressive properties of the SFRC were evaluated at 7 and 14 days. Four cylindrical specimens, at each age, were tested for the evaluation of the secant modulus of elasticity in compression and the compressive strength. The results are indicated in Table 2 (average value and the *SD*). The compressive strength and the secant modulus of elasticity in compression were determined, respectively, according to the NP EN 12390–3:2011[59] and NP EN 12390–13:2014.[60]

The properties of the SFRC under bending were also determined at 7 and 14 days. Three-point bending tests with notched beams (six specimens at 7 days and four at 14 days) were carried out according to the recommendations of *fib* Model Code 2010[58] for the evaluation of the residual flexural tensile strength parameters ($f_{R,1}$, $f_{R,2}$, $f_{R,3}$, and $f_{R,4}$ that correspond to crack mouth opening displacement, CMOD, of 0.5, 1.5, 2.5, and 3.5 mm, respectively). Figure 2 shows a sketch of the bending tests. The results are included in Table 2. The load versus crack mouth opening displacement (F-CMOD) curves are displayed in Figure 3.

The steel bar reinforcements adopted in the beams had the properties shown in Table 3, which were determined for three diameter type bars used. The yield stress and the tensile strength were determined according to the NP EN ISO 6892-1:2016.[61]

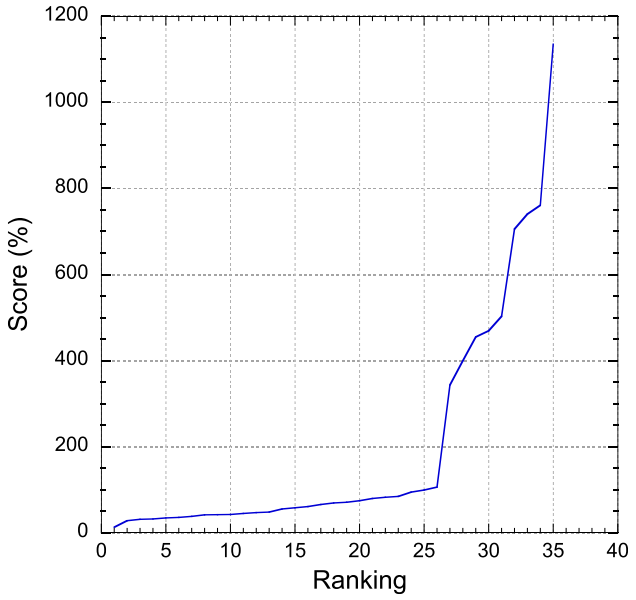


FIGURE 7 Score of participants

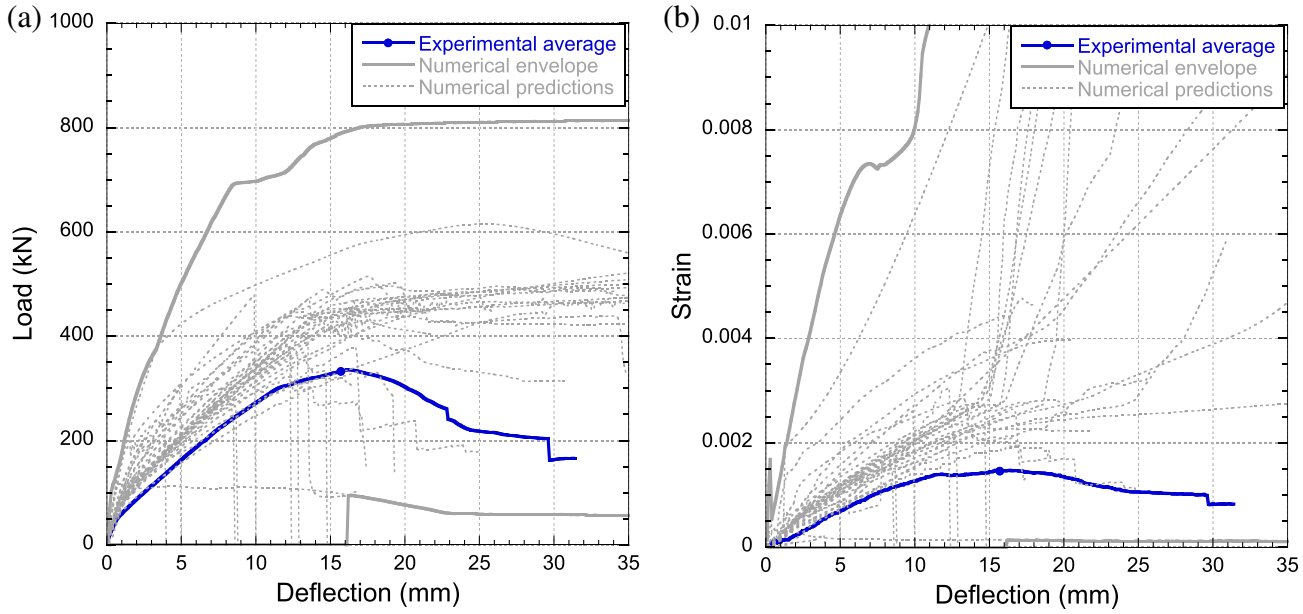


FIGURE 8 Experimental results, numerical envelope and numerical predictions of all participants of (a) load versus deflection and (b) strain versus deflection

3 | EXPERIMENTAL PROGRAM

3.1 | Test set up and monitoring system

Two twin beams were subjected to eccentric loading under displacement control of 50 μm/s at the loaded section, until failure. During the tests, deflection (displacement of the cross section at which the load is applied), load and concrete strain at the level of the longitudinal reinforcement in the loaded section were measured (see Figure 4). The strain was determined by dividing the displacement measured in a displacement transducer (LVDT) by the measuring reference length (100 mm). The LVDT for measuring the beam deflection was supported on a Japanese yoke system (see Figure 4) in order to exclude parasitic values from the displacements recorded by this LVDT.

3.2 | Results

Figure 5 displays the experimental results. Unfortunately, the record of the strain of the first beam was lost. Figure 6

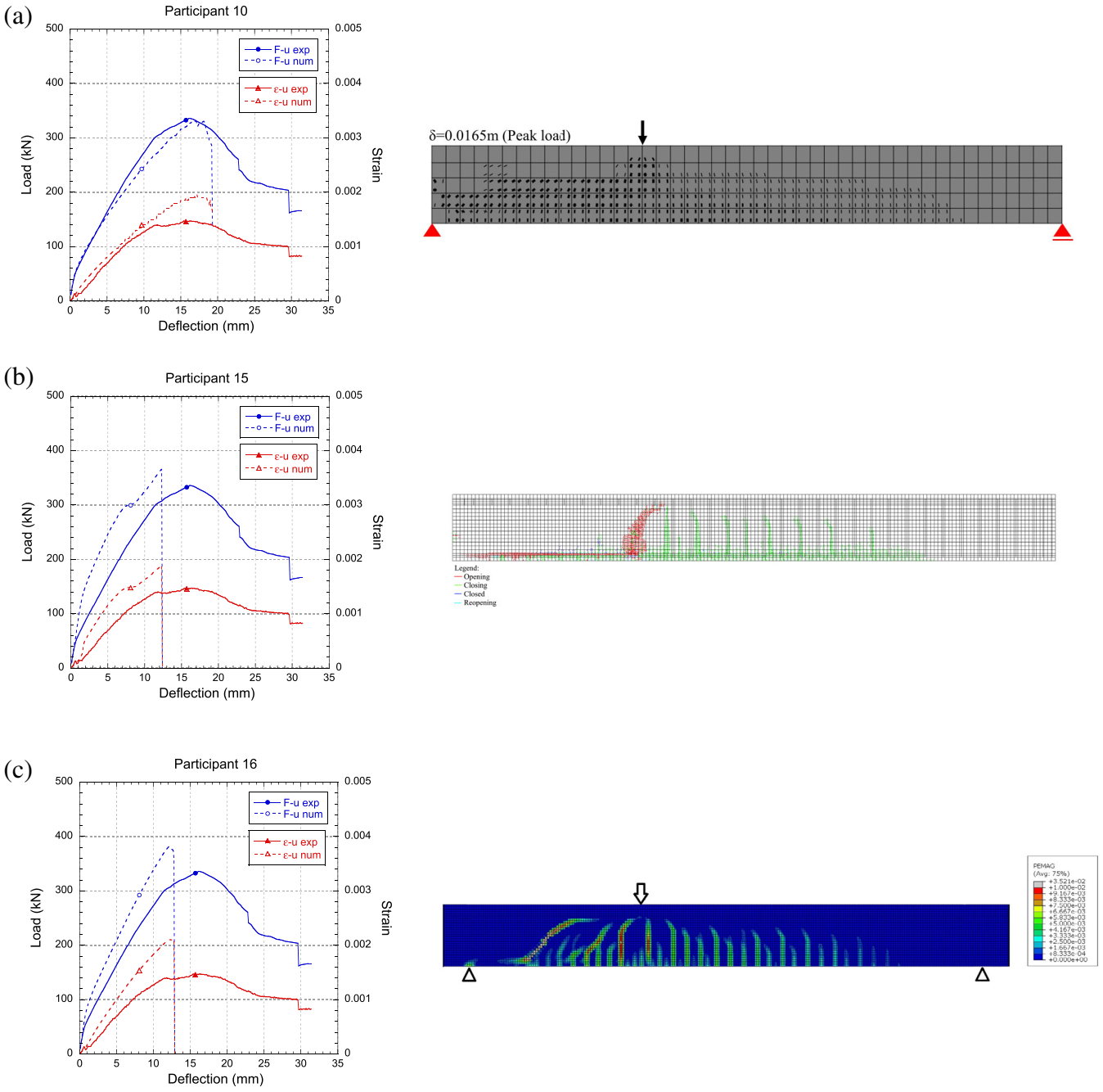


FIGURE 9 Results of the participant classified in the first three positions

represents the crack pattern at failure of both tested beams, which shows that each beam failed in shear.

4 | COMPARISON OF THE RESULTS

4.1 | Criterion for the performance level of a simulation

The predictive performance of each simulation was computed after performing the tests, according to the following methodology:

1. The average of experimental load and strain were computed from the results of the two beams.
2. The numerical results of each participant were compared with the experimental average, up to the experimental peak load. For a simulation that ended before the peak load registered experimentally, it was assumed that a brittle failure was predicted (therefore, null values were assumed up to the displacement corresponding to the peak load).
3. The error Err_{F} of the load of the numerical prediction was calculated as:

$$Err_{\mathrm{F}} = \frac{1}{n}\sum_{\kappa}\left(\frac{\left|F^{\kappa}_{\mathrm{exp}} - F^{\kappa}_{\mathrm{num}}\right|}{F^{\kappa}_{\mathrm{exp}}}\right), \tag{1}$$

where κ corresponds to the κ^{th} scan reading, $F^{\kappa}_{\mathrm{exp}}$ and $F^{\kappa}_{\mathrm{num}}$ are the experimental and the numerical values of load for record κ, respectively, and n is the total number of scan readings. An equivalent equation was used to compute the error of the strain Err_{ε}.

4. The relative error of the maximum numerical load $\Delta F/F$ was computed as:

$$\Delta F/F = \frac{\left|F^{\mathrm{max}}_{\mathrm{exp}} - F^{\mathrm{max}}_{\mathrm{num}}\right|}{F^{\mathrm{max}}_{\mathrm{exp}}}, \tag{2}$$

where $F^{\mathrm{max}}_{\mathrm{exp}}$ is the maximum load of the average of experiments and $F^{\mathrm{max}}_{\mathrm{num}}$ is the maximum load of the numerical prediction. A similar expression was used to compute the relative error of the strain $\Delta\varepsilon/\varepsilon$, considering the strain corresponding to the maximum load of experiments, $\varepsilon_{F^{\mathrm{max}}_{\mathrm{exp}}}$, and strain corresponding to the maximum load of the numerical prediction, $\varepsilon_{F^{\mathrm{max}}_{\mathrm{num}}}$, and the relative error of the deflection $\Delta u/u$, considering the corresponding $u_{F^{\mathrm{max}}_{\mathrm{exp}}}$ and $u_{F^{\mathrm{max}}_{\mathrm{num}}}$.

5. The score of each participant was calculated, considering the error of the numerical curves with respect to the average of the experiments and the relative errors of the maximum load, strain and deflection

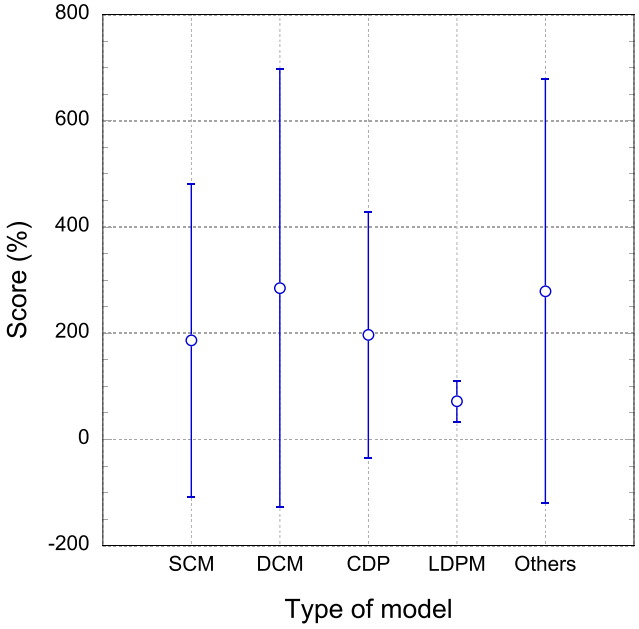


FIGURE 10 Score per classes of models, where SCM, DCM, CDP, and LDPM, respectively, stand for smeared crack model, discrete crack model, concrete damage plasticity model, and lattice discrete particle model

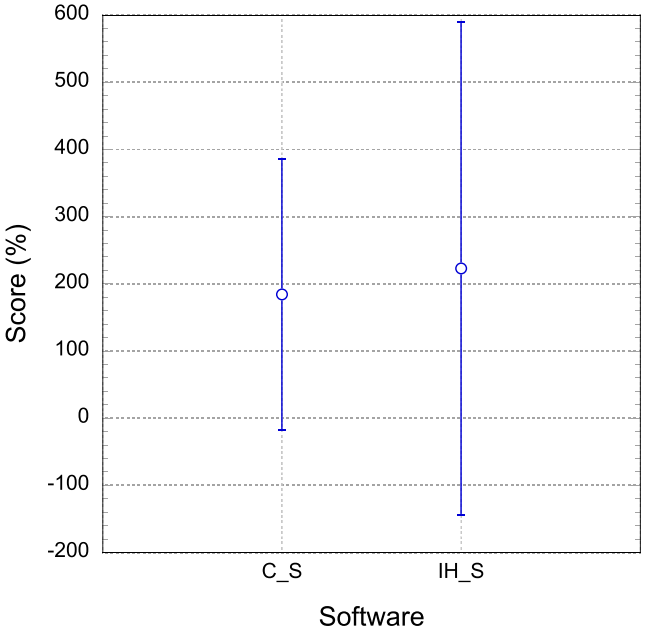


FIGURE 11 Score per type of software, where C_S and IH_S stand for, respectively, commercial and in-house Software

corresponding to the maximum load, according to the following expression:

$$Score = 0.35\,\Delta F/F + 0.15\,Err_F + 0.25\,\Delta\varepsilon/\varepsilon + 0.1Err_\varepsilon + 0.15\Delta u/u. \quad (3)$$

4.2 | Performance of the numerical simulations of the participants

A total of 37 proposals were received from 36 participants; one of them submitted two proposals. See Appendix B for the list of participants.

In the following, a random designation P_i is attributed for making reference to a generic participant i, with i = 1 to 36, for the sake of confidentiality.

Table 4 includes the predictive performance of the simulations of the 36 participants. The two models presented by one of the participants are identified by adding a and b to the corresponding P_i identification (i.e., number 12). In these results, the class of model and type of software is displayed as well, which will be analyzed in Section 5. For this purpose, the type of models indicated in the proposals were grouped in the following sets: SCM, whether fixed, multidirectional fixed or rotating cracking approaches, and formulated in a total or incremental strain basis; DCM, regardless of being supported in embedded strong discontinuities concepts, or using interface finite elements in the contour of regular finite elements; concrete damage plasticity (CDP) model; lattice discrete particle models (LDPM); and others models, based on moment-rotation, partition-of-unity, rigid-body-spring, and three-phase approaches.

Regarding the type of software used in the simulations, two groups were classified: in-house software (IH_S); and C_S.

Figure 7 shows the scores of the participants. It should be noted that the scores of participants 13 and 34 have been excluded from the graphic, as they are out of the range of results of the remaining participants.

Figure 8 shows the experimental average, the individual numerical predictions, and the envelope for the curves of load versus deflection and strain versus deflection. The results are displayed up to the deflection corresponding to the end of the experiments. Note that the curves of strain of participants 13 and 34 have been excluded from the graphic, as they are out of the range of results of the remaining participants.

Figure 9 shows the results of the participants classified in the first three positions. The numerical and experimental average curves of load versus deflection and strain versus deflection are displayed in the left part of these figures, while the crack pattern obtained at peak load is shown in the right part. Note that any reference to the calculation program is omitted for the sake of confidentiality.

The load-deflection-strain relationships and crack pattern predicted by the simulation of each participant are presented in Appendix A.

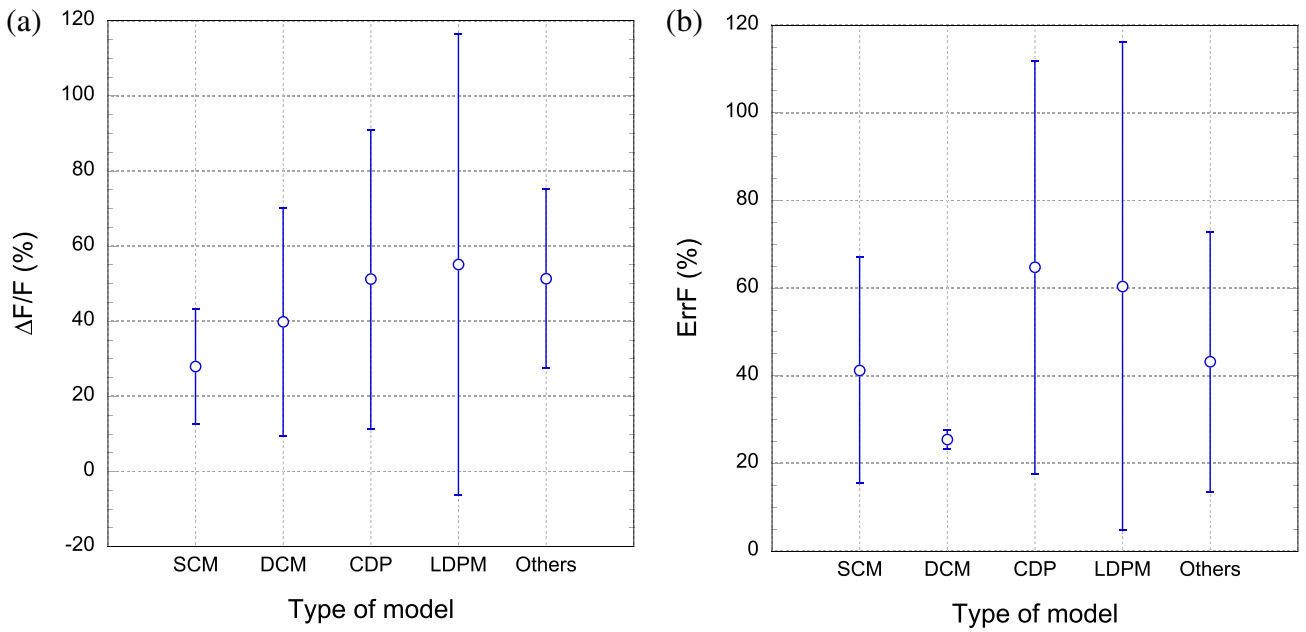


FIGURE 12 Predictive performance of the classes of models in terms of the: (a) relative error of the maximum load $\Delta F/F$ and (b) error of the load Err_F

5 | PRELIMINARY ANALYSIS OF THE RECEIVED SIMULATIONS

According to the criterion adopted to group the type of models, indicated in Section 4.2, with information provided in Table 4, five classes of models are identified from the proposals of the participants, in the following percentages:

- Smeared crack models (SCM): 17 proposals (45.9%)
- Discrete crack models (DCM): three proposals (8.11%)
- Concrete damage plasticity (CDP) model: 11 proposals (29.7%)
- Lattice discrete particle models (LDPM): two proposals (5.41%)
- Others: four proposals (10.8%)

Figure 10 shows the score (mean and *SD*) per class of models, computed from the results of the proposals using those classes. It should be noted that the lower the score, the better is the predictive performance of the simulation. Perfect simulation has a null score. For the same reason as explained in Section 4.2 for the presentation of the proposals score, the results obtained from participants 13 and 34 have been excluded from the analysis of results, as they are out of the range of results of the remaining participants.

According to the criterion adopted for grouping the type of software used in the simulations (see Section 4.2), 22 proposals (59.5%) adopted C_S and 15 proposals (40.5%) IH_S. Figure 11 shows the score per type of software.

Last, the predictive performance for each item of the evaluation Equation (3) ($\Delta F/F$, Err_F, $\Delta\varepsilon/\varepsilon$, Err_ε, $\Delta u/u$) is compared per classes of models, by considering the accuracy of a model to predict:

Err_F: the load carried by the beam up to its peak load;
Err_ε: the strain of the beam up to its peak load;
$\Delta F/F$: the beam maximum load capacity.
$\Delta u/u$: the beam deflection at its maximum load.

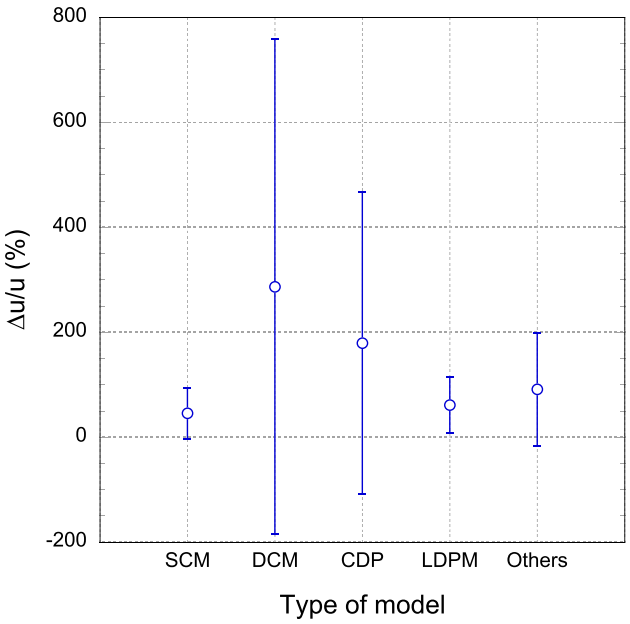


FIGURE 14 Predictive performance of the classes of models in terms of the relative error of the deflection corresponding to the maximum load $\Delta u/u$

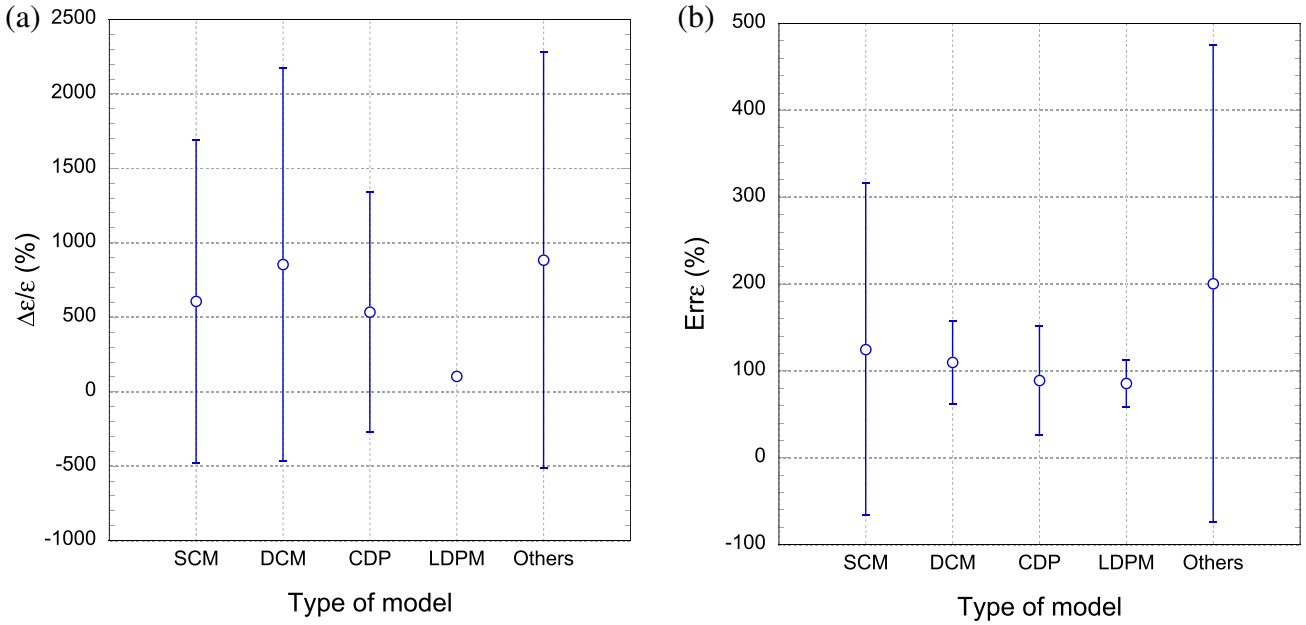


FIGURE 13 Predictive performance of the classes of models in terms of the: (a) relative error of the strain corresponding to the maximum load $\Delta\varepsilon/\varepsilon$ and (b) error of the strain Err_ε

$\Delta\varepsilon/\varepsilon$: the strain in the concrete target region at the beam's maximum load.

Figures 12–14 show the obtained results.

6 | CONCLUSIONS

This paper has presented the results of the BSC organized by the *fib* WG 2.4.1 with the purpose of providing a first assessment on the predictive performance of available FEM-based constitutive models on the simulation of real scale FRC beams failing in shear. Based on the obtained results, the following points can be highlighted:

1. The two first ranked participant teams have used SCM, though the dispersion on the predictions with this class of models was high, and was only exceeded in the DCM and the class of models designated as "others," which included moment-rotation, partition-of-unity, rigid-body-spring, and three-phase models.
2. The classification from the best to the weakest, in terms of the average predictive performance of the class of models was LDPM, SCM, CDP, others, and DCM.
3. The predictive performance of the proposals where C_S was used was better and with smaller dispersion than in the proposals where IH_S was utilized.
4. The predictive performance was also assessed in terms of load-carrying capacity of the beam up to its peak load (Err_F), the strain of the beam up to its peak load (Err_ε), beam maximum load capacity ($\Delta F/F$), beam deflection at its maximum load ($\Delta u/u$), and the strain in the concrete target region at beam maximum load ($\Delta\varepsilon/\varepsilon$). The obtained results demonstrated the SCM had the best predictions in terms of $\Delta F/F$ and $\Delta u/u$ (but almost equal to the one obtained by the LDPM for this last indicator); the DCM had the best predictions in terms of Err_F; the LDPM had the best predictions in terms of $\Delta\varepsilon/\varepsilon$ and Err_ε, but not significantly different from the predictions of CDP for this last indicator.
5. The crack pattern of the simulations of the participants in second- and third-ranking positions corresponds to a shear failure, while this failure mode is not evident in the crack pattern of the simulation of the participant in the first position.

It should be noted that the performance indicators should not be dissociated from the number of proposals per each class of models and the experience of the authors of the proposals, since in some cases the authors are those that have direct or indirect participation on the development of the software.

The authors now aim to perform a deeper analysis on the received proposals with the aim of capturing the potentialities and weaknesses of the constitutive models used for the type of structures analyzed, with the purpose of providing useful information for designers that use the types of models adopted in this BSC. Participants with the best predictive performance on the most used classes of models will be invited to collaborate with the authors on the indicated activities. Furthermore, the *fib* WG 2.4.1 seeks to provide this type of BSCs with continuity, since it is a reliable methodology for collecting comprehensive experimental programs for the assessment of the predictive performance of available and future constitutive models.

ACKNOWLEDGMENTS

The authors acknowledge the support provided by FCT through the project ICoSyTec, reference PTDC/ECI-CON/27990/2017, and PGC2018-097116-A-I00 (MCIU/AEI/FEDER, UE). In addition, they express their gratitude for the support provided by the companies Casais, for production of the beams, and CiviTest, for the execution of the specimens and the experimental tests for the characterization of the mechanical properties of the SFRC and steel bars of the conventional reinforcements of the BSC. Last but not least, they are grateful for the support from *fib* on the dissemination of the BSC.

NOTATIONS

BSC	blind simulation competition
CDP	concrete damage plasticity
CMOD	crack mouth opening displacement
C_S	commercial software
DCM	discrete crack models
FEM	finite element method
FRC	fiber-reinforced concrete
IA	inverse analysis
IH_S	in-house software
LDPM	lattice discrete particle models
LVDT	displacement transducer
Mean	average value
3PNBBT	three-point notched beam-bending tests
RPT	round panel tests
R/SFRC	steel-fiber-reinforced concrete beam with conventional longitudinal reinforcement
SCM	smeared crack models
SFRC	steel fiber-reinforced concrete
SLS	serviceability limit state
STD	standard deviation
ULS	ultimate limit state
E_{cm}	secant modulus of elasticity in compression
Err_F	error of load of the numerical prediction

Err_ε	error of strain of the numerical prediction
fcm	mean compressive strength
$f_{f,Lm}$	mean limit of proportionality
$f_{R,im}$	mean residual flexural strength corresponding to a CMOD of i mm (i = 0.5, 1.5, 2.5, and 3.5 mm)
F_{exp}^{max}	maximum load of the average of experiments
F_{exp}^{κ}	experimental value of load for record κ
F_{num}^{max}	maximum load of the numerical prediction
F_{num}^{κ}	numerical value of load for record κ
n	number of scan readings
$u_{F_{exp}^{max}}$	displacement corresponding to the maximum load of experiments
$u_{F_{num}^{max}}$	displacement corresponding to the maximum load of the numerical prediction
$\varepsilon_{F_{exp}^{max}}$	strain corresponding to the maximum load of experiments
$\varepsilon_{F_{num}^{max}}$	strain corresponding to the maximum load of the numerical prediction
$\Delta F/F$	relative error of the maximum load of the numerical prediction
$\Delta u/u$	relative error of the deflection of the numerical prediction
$\Delta\varepsilon/\varepsilon$	relative error of the strain of the numerical prediction

DATA AVAILABILITY STATEMENT

The data that support the findings of this study are available on request from the corresponding author. The data are not publicly available due to privacy or ethical restrictions.

ORCID

Joaquim Barros https://orcid.org/0000-0003-1528-757X

REFERENCES

1. Mobasher, B.; Barros, J.A.O.; Naaman, A.E.; Destree, X.; et al., "Report on design and construction of steel fiber-reinforced concrete elevated slabs", ACI 544.6R-15, Reported by ACI Committee 544, 2015.
2. Bentur A, Mindess S. Fibre reinforced cementitious composites. 2nd ed. Oxfordshire, UK: Francis & Taylor, 2007.
3. Craig R. Malmo's constructions starts. Tunneling Trenchless Construct. 2006;12–14.
4. Craig R. Dartford cable tunnel. Tunneling Trenchless Construct. 2004;17–19.
5. Gambarova, P., "Overview of recent advancements in FRC knowledge and applications with specific reference to high temperature" Proceedings, RILEM Technical Meeting, pp. 125–140, 2004.
6. Balaguru PN, Shah SP. Fiber reinforced cement composites. Singapore: McGraw-Hill International Editions, Civil Engineering Series, 1992.
7. Kaufmann W, Amin A, Beck A, Lee M. Shear transfer across cracks in steel fibre reinforced concrete. Eng Struct. 2019;186:508–524. https://doi.org/10.1016/j.engstruct.2019.02.027.
8. Matos LMP, Barros JAO, Ventura-Gouveia A, Calçada R. Constitutive model for fibre reinforced concrete by coupling the fibre and aggregate interlock resisting mechanisms. Cem Concr Compos J. 2020;111:103618. https://doi.org/10.1016/j.cemconcomp.2020.1036.
9. Cavagnis F, Ruiz MF, Muttoni A. Shear failures in reinforced concrete members without transverse reinforcement: An analysis of the critical shear crack development on the basis of test results. Eng Struct. 2015;103:157–173. https://doi.org/10.1016/j.engstruct.2015.09.015.
10. Foster, S.J.; Lee, G.G.; Htut, T.N.S. "Radiographic imaging for the observation of modes I and II fracture in fibre reinforced concrete" Paper presented at: The 6th International Conference on Fracture Mechanics of Concrete and Concrete Structures, 2007, p.8. URL https://framcos.org/FraMCoS-6/410.pdf
11. Jang S-J, Jeong G-Y, Yun H-D. Use of steel fibers as transverse reinforcement in diagonally reinforced coupling beams with normal- and high-strength concrete. Construct Build Mater. 2018, ISSN 09500618;187:1020–1030. https://doi.org/10.1016/j.conbuildmat.2018.08.063.
12. Adebar P, Mindess S, St-Pierre D, Olund B. Shear tests of fiber concrete beams without stirrups. ACI Struct J. 1997;94(1):68–76.
13. Kwak Y-K, Eberhard MO, Kim W-S, Kim J. Shear strength of steel fiber-reinforced concrete beams without stirrups. ACI Struct J. 2002;99(4):530–538.
14. Minelli F, Plizzari GA, Vecchio FJ. Influence of steel fibers on full-scale RC beams under shear loading. In: Carpinteri A, Gambarova PG, Ferro G, Plizzari GA, editors. Fracture mechanics of concrete structures–High performance concrete, brick-masonry and environmental aspects. London: Taylor and Francis, 2007; p. 1523–1531.
15. Aoude H, Belghiti M, Cook WD, Mitchell D. Response of steel fiber-reinforced concrete beams with and without stirrups. ACI Struct J. 2012;109(3):359–368.
16. Conforti A, Minelli F, Plizzari GA. Wide-shallow beams with and without steel fibres: A peculiar behaviour in shear and flexure. Compos Part B Eng. 2013;51:282–290.
17. Singh B, Jain K. Appraisal of steel fibers as minimum shear reinforcement in concrete beams. ACI Struct J. 2014;111(5):1191–1202.
18. Amin A, Foster SJ. Shear strength of steel fibre reinforced concrete beams with stirrups. Eng Struct. 2016;111:323–332.
19. Frazão CMV, Barros JAO, Camões AFLL, Alves A, Rocha L. Corrosion effects on pullout behavior of hooked steel fibers in self-compacting concrete. Cem Concr Res. 2016;79:112–122. https://doi.org/10.1016/j.cemconres.2015.09.005.
20. Frazão, C.M.V., Recycled steel fiber reinforced concrete for structural elements subjected to chloride attack: Mechanical and durability performance, PhD thesis, University of Minho, 2019.
21. Nobili A, Lanzoni L, Tarantino AM. Experimental investigation and monitoring of a polypropylene-based fiber reinforced concrete road pavement. Construct Build Mater. 2013;47:888–895.
22. Chen Y, Cen G, Cui Y. Comparative analysis on the anti-wheel impact performance of steel fiber and reticular polypropylene synthetic fiber reinforced airport pavement concrete under elevated temperature aging environment. Construct Build Mater. 2018, ISSN 09500618;192:818–835. https://doi.org/10.1016/j.conbuildmat.2018.10.175.

23. Yang M, Shin H-O, Yoo D-Y. Benefits of using amorphous metallic fibers in concrete pavement for long-term performance. Arch Civil Mech Eng. 2017, ISSN 16449665;17(4): 750–760. https://doi.org/10.1016/j.acme.2017.02.010.
24. Conforti A, Tiberti G, Plizzari GA, Caratelli A, Meda A. Precast tunnel segments reinforced by macro-synthetic fibers. Tunnelling Underground Space Technol. 2017, ISSN 08867798;63: 1–11. https://doi.org/10.1016/j.tust.2016.12.005.
25. Soetens, T., Design models for the shear strength of prestressed precast steel fibre reinforced concrete girders, PhD thesis, Gent University, 2015.
26. Gonilha JA, Barros JAO, Correia JR, et al. Static, dynamic and creep behaviour of a full-scale GFRP-SFRSCC hybrid footbridge. Compos Struct. 2014;118:496–509, ISSN 02638223. https://doi.org/10.1016/j.compstruct.2014.08.009.
27. Barros, J.A.O., "Fiber reinforced concrete and glass fibre reinforced polymer systems for the development of more sustainable construction systems", Paper presented at: 9th RILEM International Symposium on Fiber Reinforced Concrete, BEFIB 2016, Vancouver, Canada, 2016.
28. Abrishambaf A, Cunha V, Barros JAO. The influence of fibre orientation on the post-cracking tensile behaviour of steel fibre reinforced self-compacting concrete. Fract Struct Integr J. 2016; 31(1):38–53.
29. Ferrara L, Meda A. Relationship between fibre distribution, workability and the mechanical properties of SFRC applied to precast roof elements. Mater Struct. 2006;39:411–420.
30. Ozyurt N, Mason TO, Shah SP. Correlation of fibre dispersion, rheology and mechanical performance of FRCs. Cem Concr Compos. 2007;29(2):70–79.
31. Ferrara L, Ozyurt N, di Prisco M. High mechanical performance of fibre reinforced cementitious composites: The role of -casting-flow induced- fibre orientation. Mater Struct. 2011;44: 109–128.
32. Gudzulic V, Dang T, Meschke G. Computational modeling of fiber flow during casting of fresh concrete. Comput Mech. 2018;63(6):1111–1129.
33. Carvalho MR, Barros JAO, Zhang Y, Dias-da-Costa D. A computational model for simulation of steel fibre reinforced concrete with explicit fibres and crack. Comput Methods Appl Mech Eng. 2020;363:112879. https://doi.org/10.1016/j.cma.2020.112879.
34. Chi Y, Yu M, Huang L, Xu L. Finite element modeling of steel-polypropylene hybrid fiber reinforced concrete using modified concrete damaged plasticity. Eng Struct. 2017;148:23–35.
35. Zhan Y, Meschke G. Adaptive crack modeling with interface solid elements for plain and fiber reinforced concrete structures. Materials. 2017;10(7):771.
36. Dancygier AN, Berkover E. Cracking localization and reduced ductility in fiber-reinforced concrete beams with low reinforcement ratios. Eng Struct. 2016;111:411–424.
37. Teixeira MDE, Barros JAO, Cunha VMCF, Moraes-Neto BN, Ventura-Gouveia A. Numerical simulation of the punching shear behaviour of self-compacting fibre reinforced flat slabs. Construct Build Mater J. 2015;74:25–36. https://doi.org/10.1016/j.conbuildmat.2014.10.003.
38. Deluce JR, Lee SC, Vecchio FJ. Crack model for steel fiber-reinforced concrete members containing conventional reinforcement. ACI Struct J. 2014;111(1):93–102. https://doi.org/10.14359/51686433.
39. Cunha VMCF, Barros JAO, Sena-Cruz JM. A finite element model with discrete embedded elements for fibre reinforced composites. Comput Struct J. 2012;94-95:22–33.
40. Oliver J, Mora DF, Huespe AE, Weyler R. A micromorphic model for steel fiber reinforced concrete. Int J Solids Struct. 2012;49(21):2990–3007.
41. Lee SC, Cho JY, Vecchio FJ. Diverse embedment model for steel fiber-reinforced concrete in tension: Model verification. ACI Mater J. 2011;108(5):526–535. https://doi.org/10.14359/51685787.
42. Seow PEC, Swaddiwudhipong S. Modeling of steel fiber-reinforced concrete under multi-axial loads. Cem Concr Res. 2006;36:1354–1361.
43. Padmarajaiah SK, Ramaswamy A. A finite element assessment of flexural strength of prestressed concrete beams with fibre reinforcement. Cem Concr Compos. 2002;24:229–241.
44. Vorel J, Kabele P. Inverse analysis of traction-separation relationship based on sequentially linear approach. Comput Struct. 2019;212:125–136.
45. Soltanzadeh F, Cunha VMCF, Barros JAO. Assessment of different methods for characterization and simulation of post-cracking behavior of self-compacting fiber reinforced concrete. Construct Build Mater J. 2019;227:116704. https://doi.org/10.1016/j.conbuildmat.2019.116704.
46. Salehian H, Barros JAO. Assessment of the performance of steel fibre reinforced self-compacting concrete in elevated slabs. Cem Concr Compos. 2015;55:268–280. https://doi.org/10.1016/j.cemconcomp.2014.09.016.
47. Rots JG, Nauta P, Kusters GMA, Blaauwendraad J. Smeared crack approach and fracture localization in concrete. HERON. 1985;30(1):1–48.
48. Rots, J.G., "Computational modeling of concrete fracture", PhD thesis, Delft University of Technology, 1988.
49. Pruijssers A.F., "Description of the stiffness relation or mixed-mode fracture problems in concrete using the rough-crack model of Walraven", TU-Delft Report, Department of Civil Engineering, No. 5–28-2, 1985.
50. Cervenka V.; Pukl H.; Eligehausen R., "Computer simulation of anchoring technique and design of concrete structures", Proceedings Second International Conference on Computer Aided Analysis And Design Of Concrete Structures, Zell am See, Austria, 1–19, 1990.
51. Rots JG, de Borst R. Analysis of mixed-mode fracture in concrete. J Eng Mech, ASCE. 1987;113(11):1739–1758.
52. Ventura-Gouveia A, Barros JAO, Azevedo AFM. Crack constitutive model for the prediction of punching failure modes of fiber reinforced concrete laminar structures. Comput Concr. 2011;8(6):735–755.
53. Vecchio FJ. Non-linear finite element analysis of reinforced concrete: At the crossroads? Struct Concr. 2001;2:201–212.
54. Collins MP, Vecchio FJ, Mehlhorn G. An international competition to predict the response of reinforced concrete panels. Canadian J Civil Eng. 1985;12:624–644.
55. Foster SJ, Agarwal A, Amin A. Design of SFRC beams for shear using inverse analysis for determination of residual tensile strength. Struct Concr. 2018;19:129–140.

56. Cuenca E, Conforti A, Minelli F, Plizzari GA, Gregori JN, Serna P. A material-performance-based database for FRC and RC elements under shear loading. Mater Struct. 2018;51(11): 1130–1137.
57. Barros JAO, Foster S. An integrated approach for predicting the shear capacity of fibre reinforced concrete beams. Eng Struct J. 2018;174:346–357. https://doi.org/10.1016/j.engstruct.2018.07.071.
58. fib Model Code 2010: *fib* Model Code for Concrete Structures 2010.
59. NP EN 12390–3:2011. Testing hardened concrete-Part 3: Compressive strength of test specimens.
60. NP EN 12390–13:2014. Testing hardened concrete-Part 13: Determination of secant modulus of elasticity in compression.
61. NP EN ISO 6892-1:2016. Metallic materials-Tensile testing - Part 1: Method of test at room temperature.

AUTHOR BIOGRAPHIES



Joaquim A. O. Barros, Full Professor ISISE, Institute of Science and Innovation for Bio-Sustainability (IB-S), Department of Civil Engineering, University of Minho, 4800-058 Guimarães, Portugal.



Beatriz Sanz, Associate Professor, Department of Materials Science, Technical University of Madrid, ETSI Caminos, Canales y Puertos, 28040 Madrid, Spain.



Petr Kabele, Czech Technical University in Prague, Czech Republic.



Rena C. Yu, University of Castilla-La Mancha, Spain.



Günther Meschke, Institute for Structural Mechanics, Ruhr University Bochum, Germany.



Jaime Planas, Technical University of Madrid, Spain.



Vitor Cunha, ISISE, Institute of Science and Innovation for Bio-Sustainability (IB-S), Department of Civil Engineering, University of Minho, Portugal.



Antonio Caggiano, Technische Universität Darmstadt, Germany.



Nilüfer Ozyurt, Bogazici University, Turkey.



Ventura Gouveia, Polytechnic Institute of Viseu, Portugal.



Ab van den Bos, DIANAFEA, The Netherlands.



Elisa Poveda, University of Castilla-La Mancha, Spain.



Erez Gal, Ben-Gurion University of Negev, Israel.



Jan Cervenka, Cervenka Consulting s.r.o., Czech Republic.



Gerrit E. Neu, Institute for Structural Mechanics, Ruhr University Bochum, Germany.



Pierre Rossi, University of Eiffel, France.



Daniel Dias-da-Costa, The University of Sydney, Australia.



Peter K. Juhasz, Budapest University of Technology and Economics, Hungary.



David Cendón, Associate Professor, Department of Materials Science, Technical University of Madrid, ETS de Ingenieros de Caminos, Madrid, Spain.



Gonzalo Ruiz, University of Castilla-La Mancha, Spain.



Tiago Valente, CiviTest-Pesquisa de Novos Materiais para a Engenharia Civil, Portugal.

How to cite this article: Barros J, Sanz B, Kabele P, et al. Blind competition on the numerical simulation of steel-fiber-reinforced concrete beams failing in shear. *Structural Concrete*. 2020;1–29. https://doi.org/10.1002/suco.202000345

APPENDIX A.: RESULTS OF THE PARTICIPANTS

Figures A1–A10 show the results for each participant. The numerical and experimental average curves of load versus deflection and strain versus deflection are displayed in the left part of each figure. Note that for a better comparison of results, the scale of load and deflection has been maintained the same in all the figures. The crack pattern obtained at peak load is shown in the right part of the figures.

APPENDIX B.: PARTICIPANTS

The list of participants and their affiliation is included below. The authors thank them for their participation in the competition.

Alejandro Nogales,[1] Nikola Tošić,[2] Albert de la Fuente[21]: Smart Engineering Ltd., UPC Spin-Off, Barcelona, Spain[2];Civil and Environmental Engineering Department, Universitat Politècnica de Catalunya, Barcelona, Spain.

Alexander Kagermanov[11]: University of Applied Science Rapperswil, Switzerland.

Antonio A. Cristian[11]: Technical University of Civil Engineering of Bucharest.

Barzin Mobasher,[1] Devansh Deepak Patel,[1] Chidchanok Pleesudjai[11]: Material Model ASU Team.

Camille A. Issa,[1] Najwa Hani[11]: Lebanese American University.

Christoph Betschoga,[1] Michael Huß,[1] Yolcu Sever,[1] Nguyen Duc Tung[11]: Institute of Structural Concrete, Graz University of Technology, Graz, Austria.

Dong Xiang[11]: Tongji University, China.

George Markou[11]: Faculty of Engineering, University of Pretoria, Hatfield, South Africa.

Gerrit E. Neu,[1] Michael Hofmann,[1] Günther Meschke[11]: Institute for Structural Mechanics, Ruhr University of Bochum, Germany.

Gili L. Sherzer,[1] Younes F. Alghalandis,[1] Karl Peterson,[1] Giovanni Grasselli[11]: University of Toronto, Canada.

Giulio Zani,[1] Matteo Colombo,[1] Marco di Prisco[11]: Politecnico di Milano, Department of Civil and Environmental Engineering.

Hiroki Ogura,[1] Minour Kunieda[21]: Shimizu Corporation, Japan,[2]Gifu University, Japan.

Inkyu Rhee,[1] Jae-Min Kim[11]: Department of Civil Engineering, Chonnam National University, Gwangju, South Korea.

Jaime Planas,[1] Beatriz Sanz,[1] José M. Sancho[21]: Dep. Ciencia de Materiales, ETS de Ingenieros de Caminos, Canales y Puertos, Universidad Politécnica de Madrid, Madrid, Spain,[2]Dep. Estructuras de Edificación, ETS Arquitectura, Universidad Politécnica de Madrid, Madrid, Spain.

Jan Červenka[11]: Červenka Consulting.

Jia-Qi Yang,[1] Zhiyuan Li[1], Peizhao Zhou,[1] Chongfeng Xie[11]: Department of Civil Engineering, Tsinghua University, Beijing, China.

José Joaquín Ortega[11]: Universidad de Castilla-La Mancha, Spain.

Josef Landler,[1] Sören Faustmann,[1] Oliver Fischer[11]: Technical University of Munich, Department of Civil, Geo and Environmental Engineering, Munich, Germany.

Lex van der Meer,[1] Kris Riemens,[1] Srinidhi Ramadas,[1] Yue Dai[11]: ABT, The Netherlands.

Luís M.P. Matos,[1] António V. Gouveia[21]: Department of Civil Engineering, University of Minho,[2]Department of Civil Engineering, Polytechnic Institute of Viseu.

Marcos A. da Silva,[1] Luiz C. de Almeida,[1] Leandro Mouta Trautwein[11]: Universidade Estadual de Campinas, School of Civil Engineering, Architecture and Urbanism, Laboratório de Modelagem Estructural e Monitoração, Campinas-SP, Brazil.

Mário Pimentel,[1] Rui Valente[11]: University of Porto, Faculty of Engineering, Porto, Portugal.

Mladena Lukovic,[1] Dawei Gu,[1] Erik Schlangen[11]: TU Delft, The Netherlands.

Mohmaed Hamza,[1] Hamed Salem[21]: Applied Science International, Cairo, Egypt,[2]Structural Engineering Department, Cairo University, Egypt.

Monday Isojeh[11]: Hatch Limited.

Osvaldo L. Manzoli,[1] Luís A.G. Bitencourt Jr.,[2] Yasmin T. Trindade[21]: São Paulo State University, Department of Civil Engineering, Bauru-SP, Brazil,[2]University of São Paulo, Department of Structural and Geotechnical Engineering, São Paulo-SP, Brazil.

Peter K. Juhasz,[1] Peter Schaul[11]: JPK Static Ltd., Department of Construction Materials and Technologies, Budapest University of Technology and Economics.

Pim van der Aa,[1] Ab van den Bos[11]: Diana FEA BV.

Rafael A. Sanabria[11]: Universidade Estadual de Campinas, Laboratorio de Modelagem Estrutural e Monitoração, Brazil.

Rutger Vrijdaghs[11]: Department of Civil Engineering, KU Leuven, Belgium.

Saeid Mehrpay,[1] Tamon Ueda[21]: Hokkaido University, Japan,[2]Shenzhen University, PR China.

Shen Le,[1,2] Ding Miao,[1,2] Yang Bo[1,21]: School of Civil Engineering, Chongquing, China,[2]Key Laboratory of New Technology for Construction of Cities in Mountain Area, Chongquing University, China.

Song Jin,[1] Yating Tai,[1] Yun Tian,[1] Chenghuan Lin,[1] Xiyao Zhao,[1] Meng Zhang,[1] Qingqing Wu,[1] Jikai Zhou[11]:

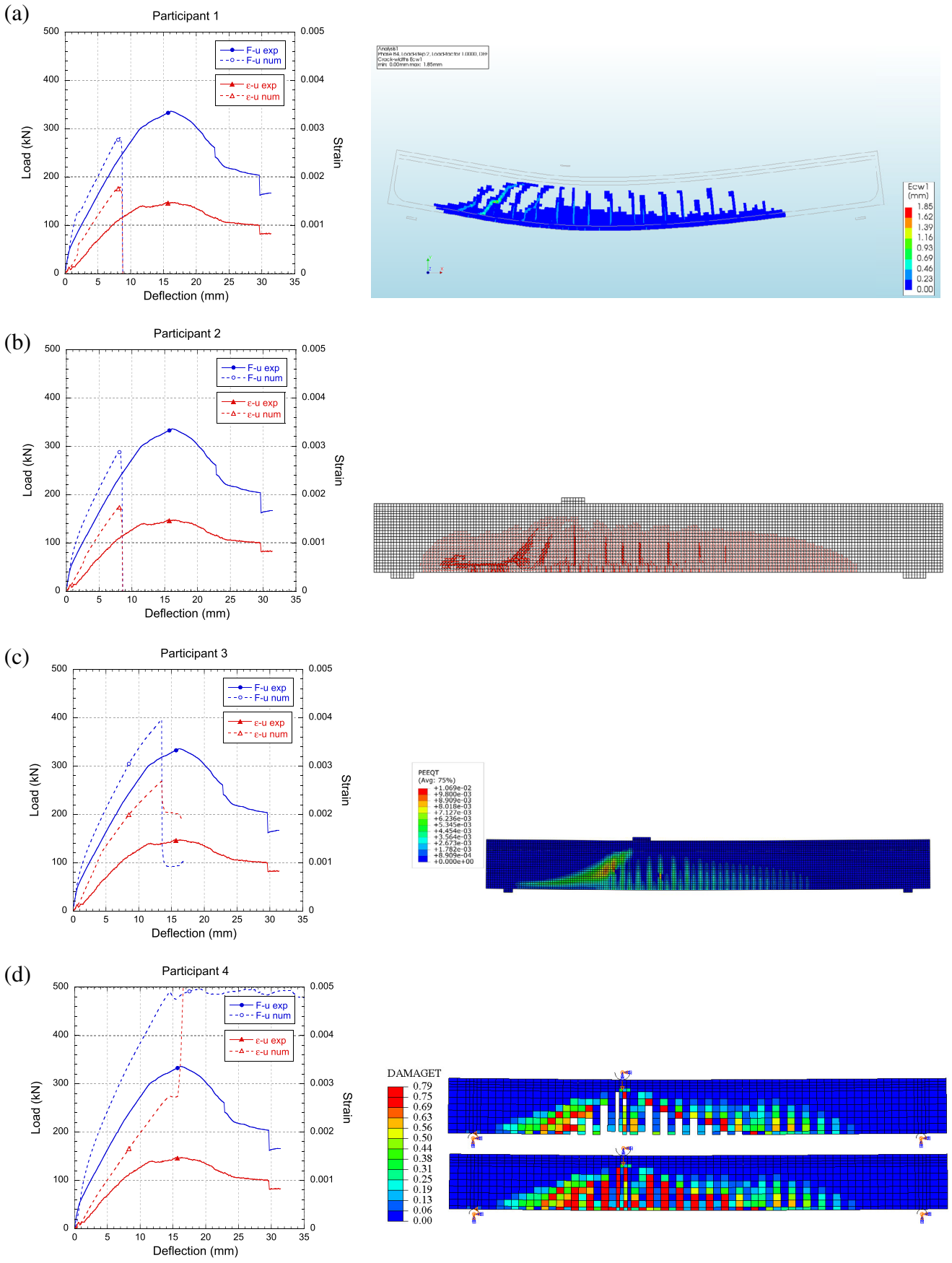


FIGURE A1 Results of participants 1–4

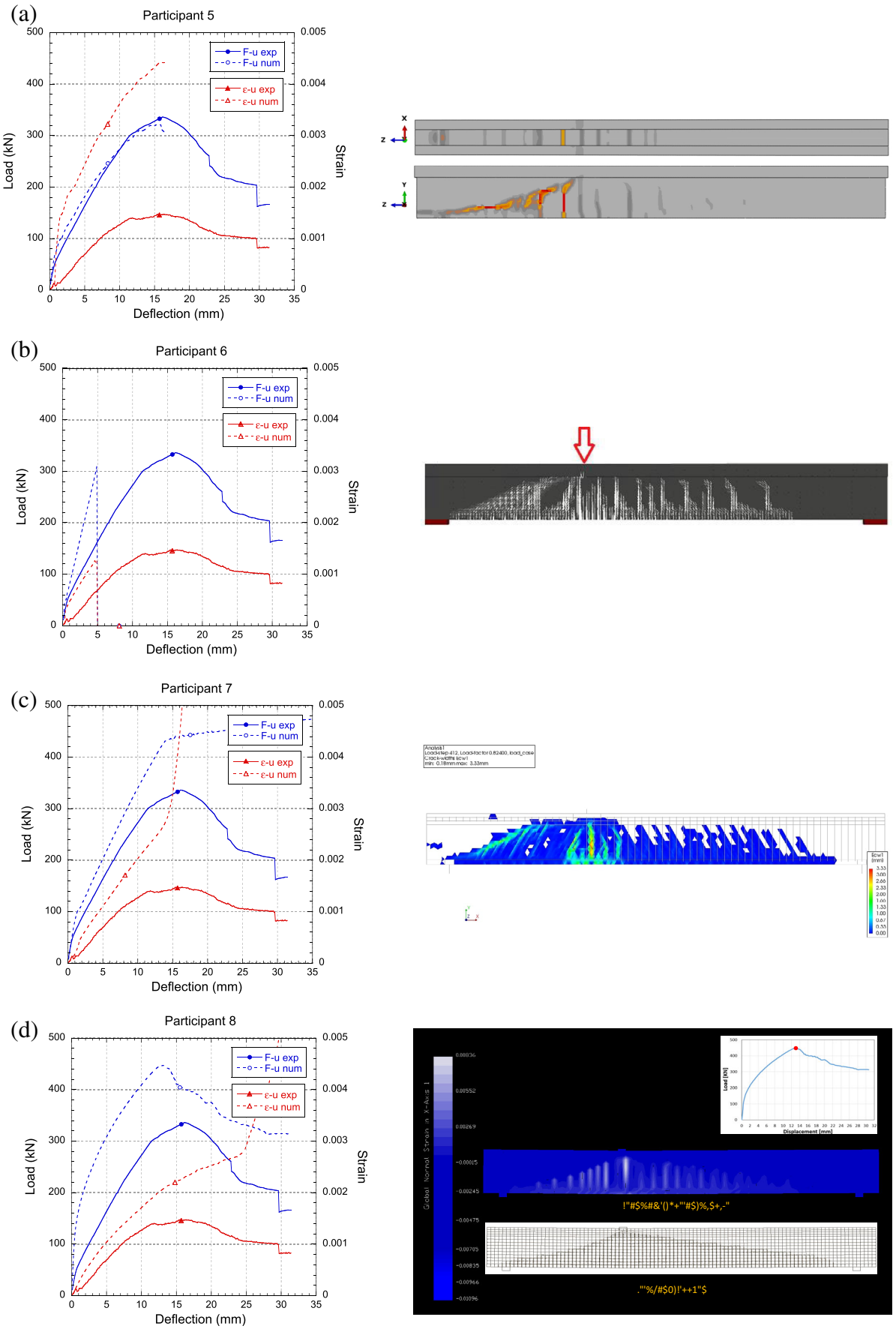


FIGURE A2 Results of participants 5–8

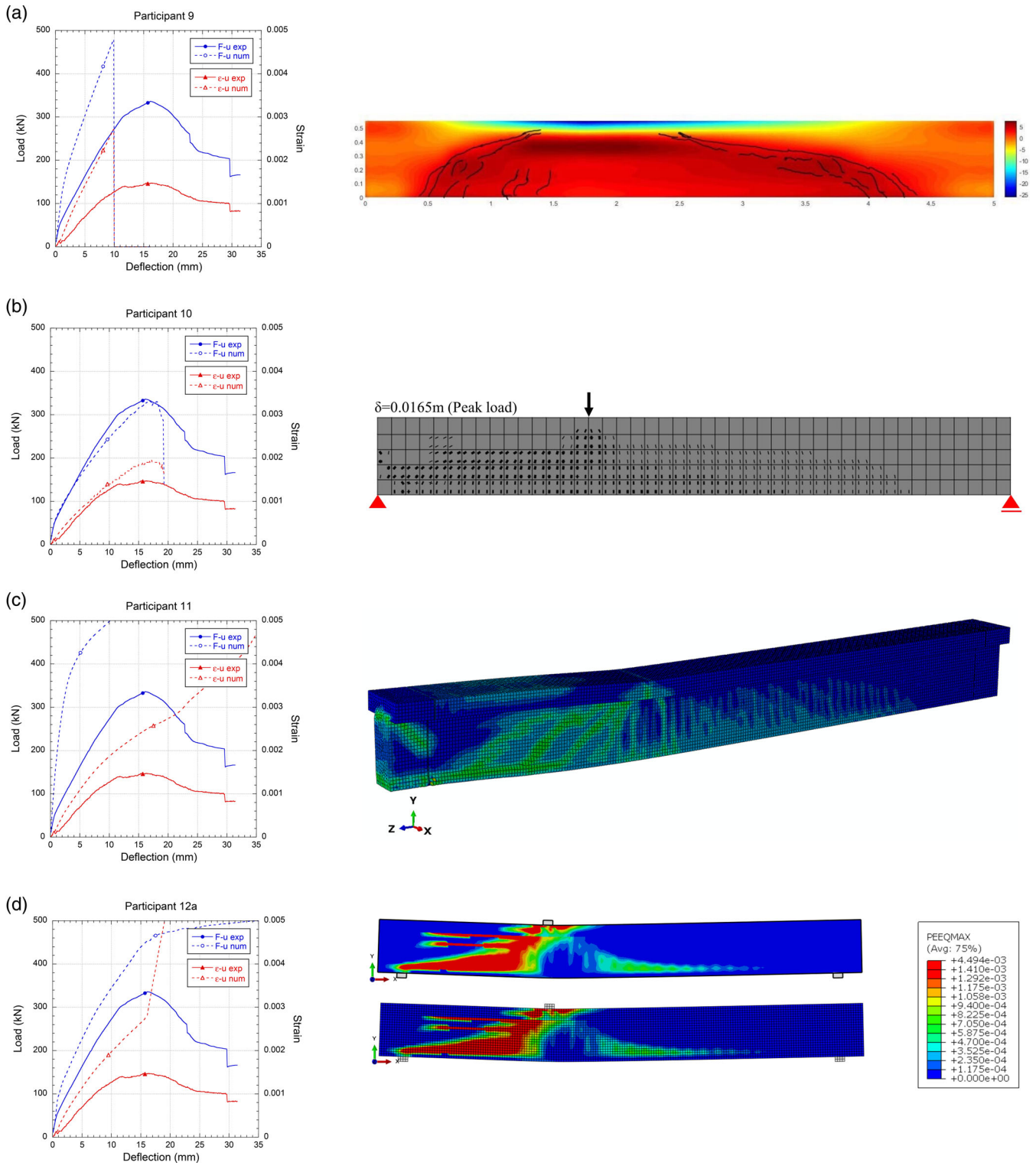


FIGURE A3 Results of participants 9–12a

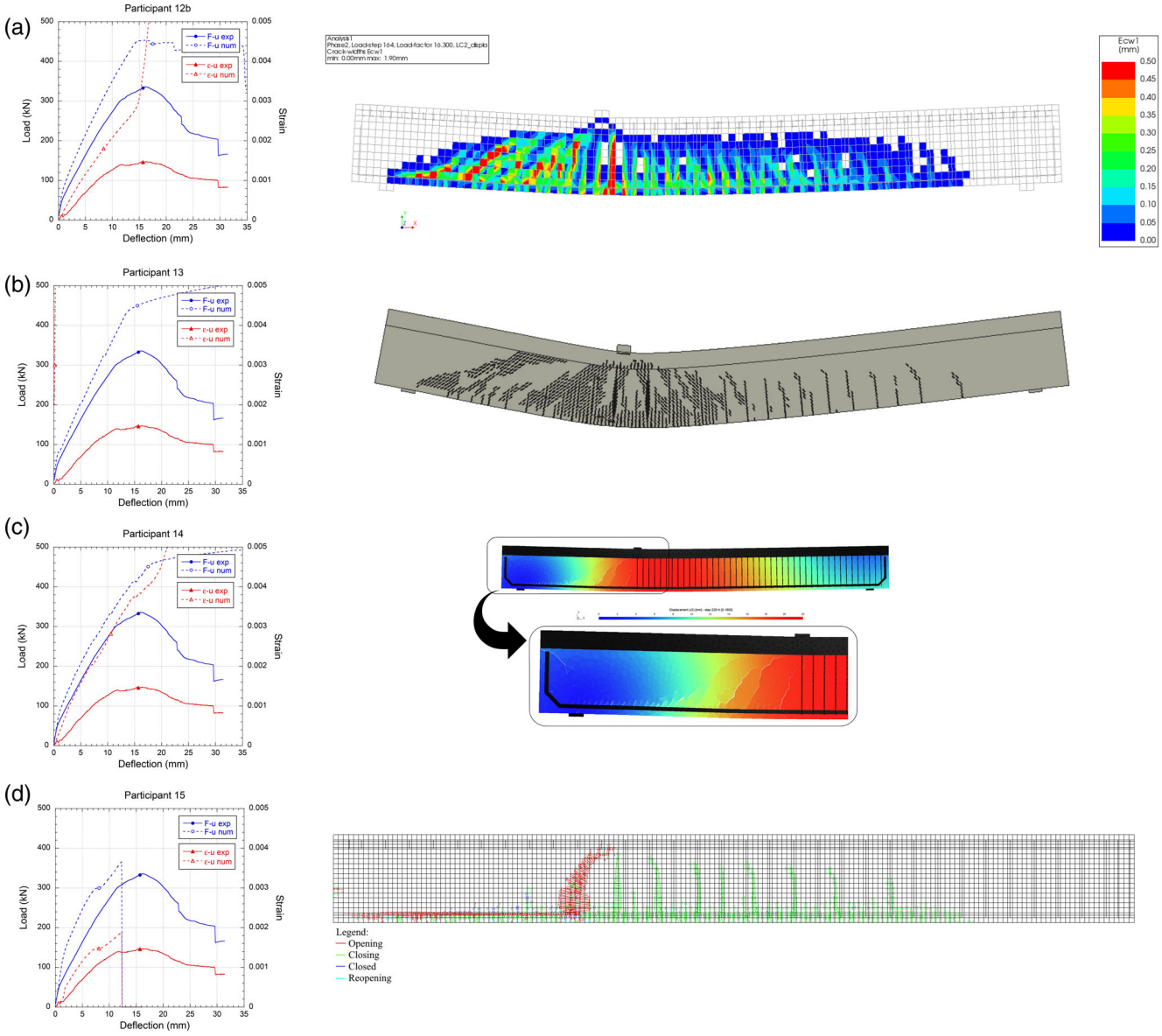


FIGURE A4 Results of participants 12b–15

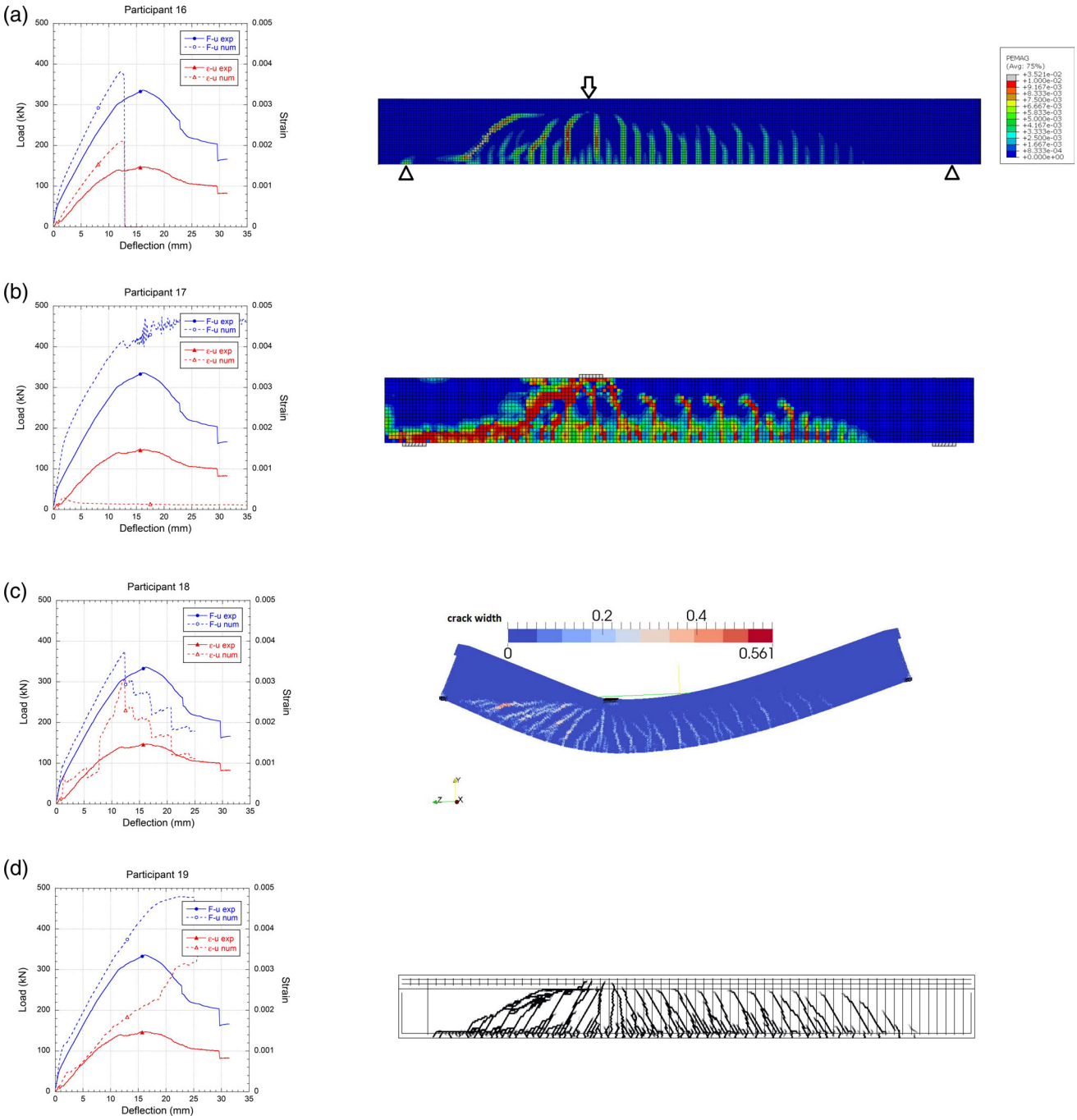


FIGURE A5 Results of participants 16–19

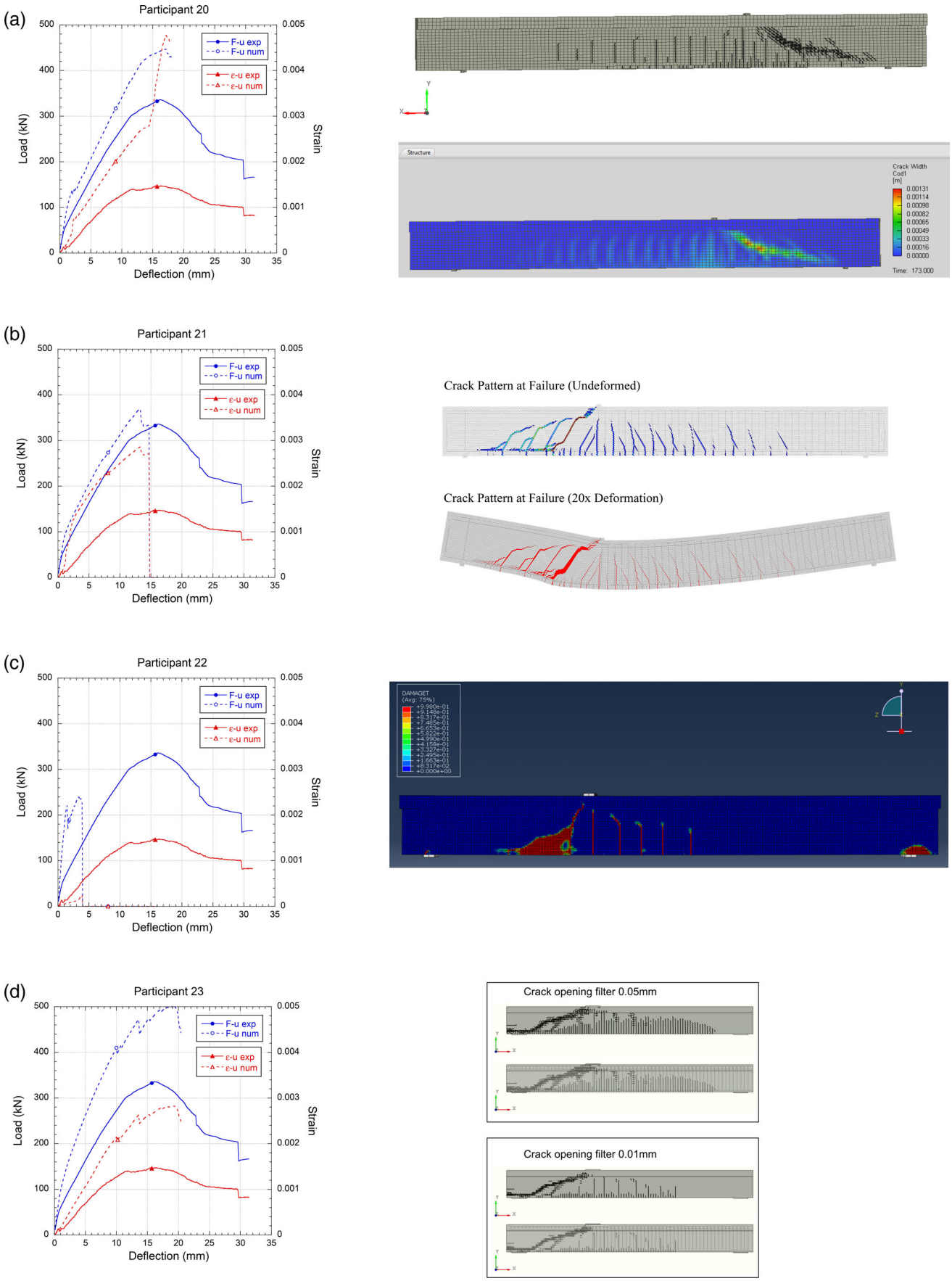


FIGURE A6 Results of participants 20–23

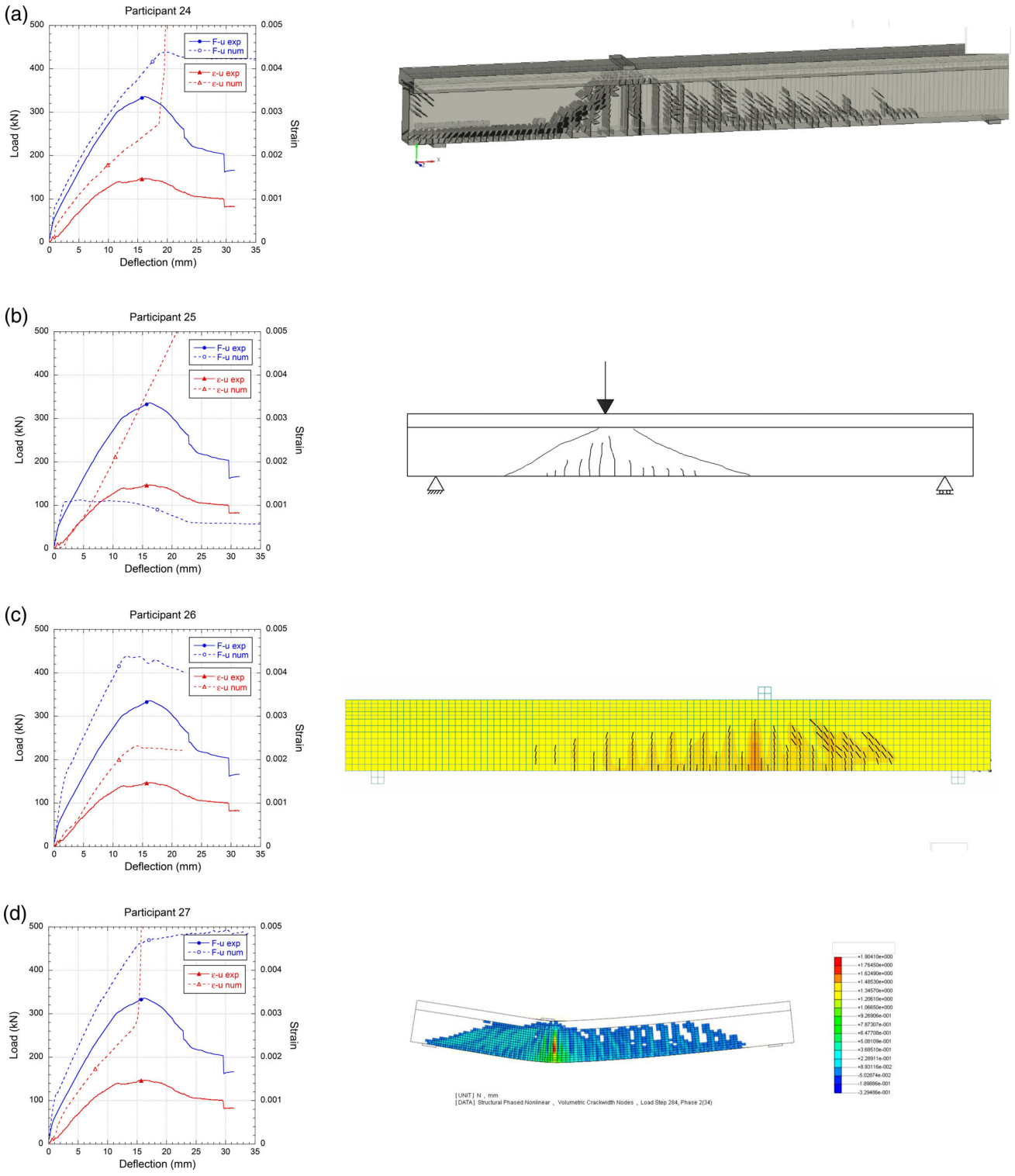


FIGURE A7 Results of participants 24–27

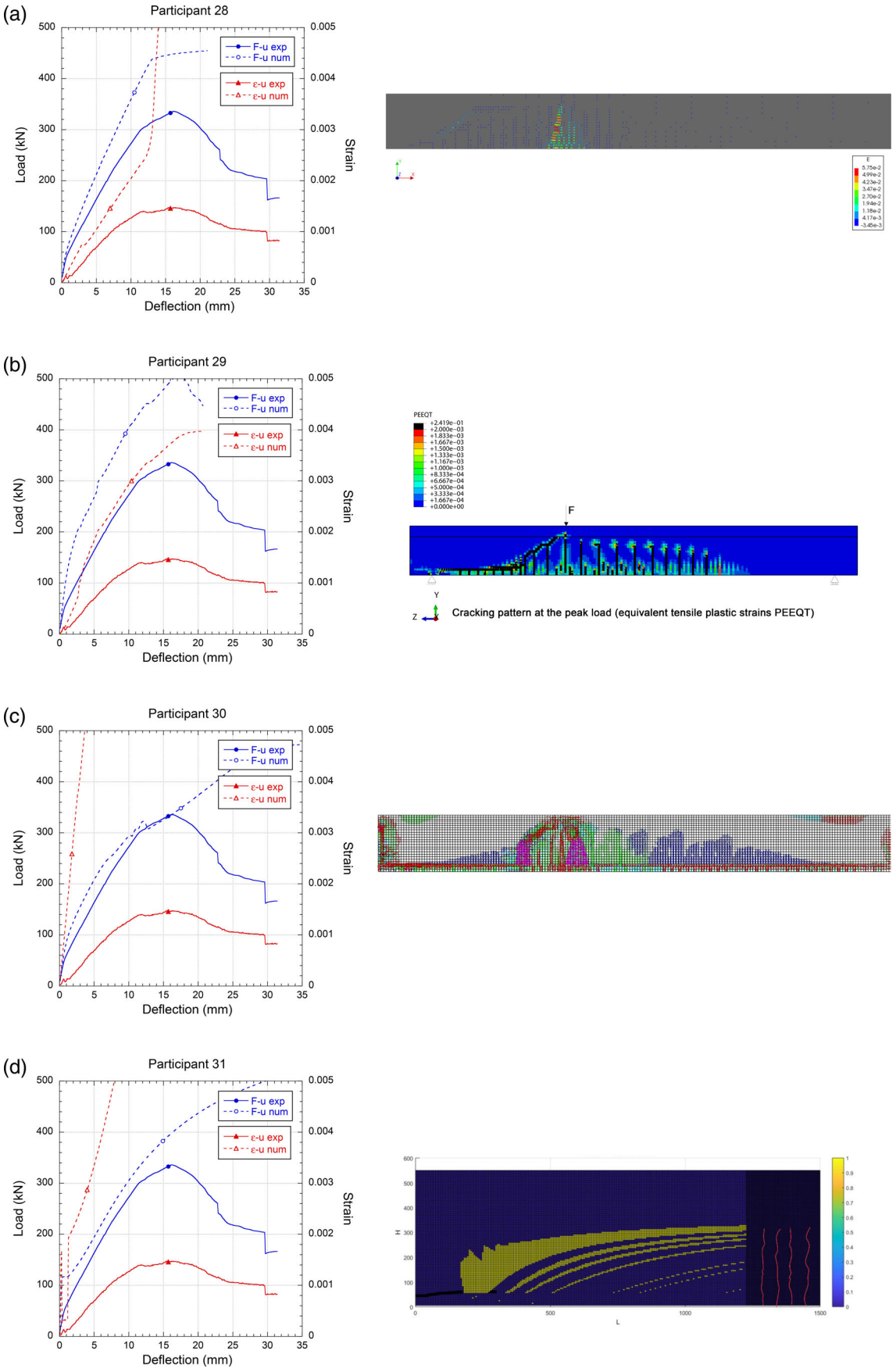


FIGURE A8 Results of participants 28–31

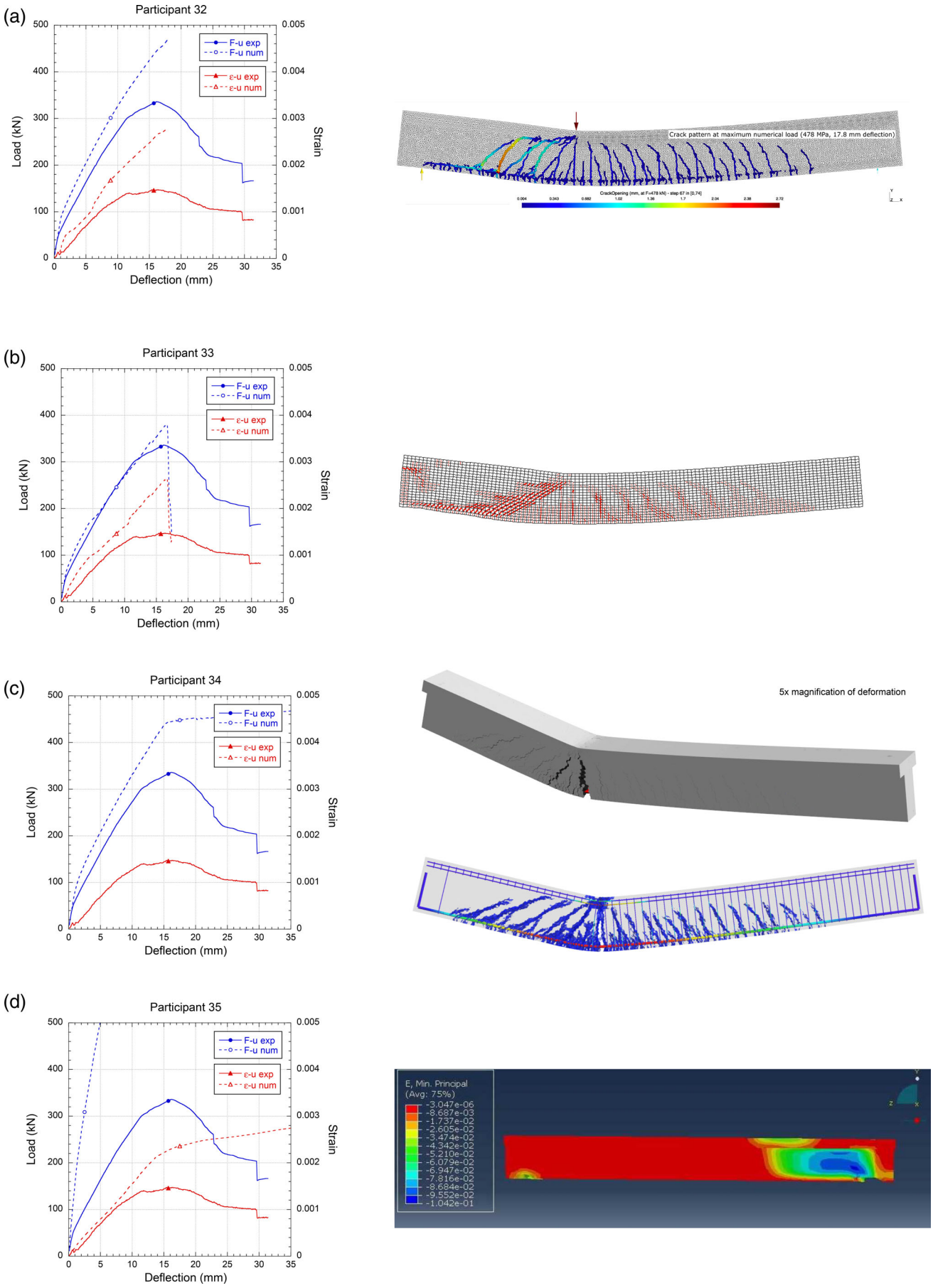


FIGURE A9 Results of participants 32–35

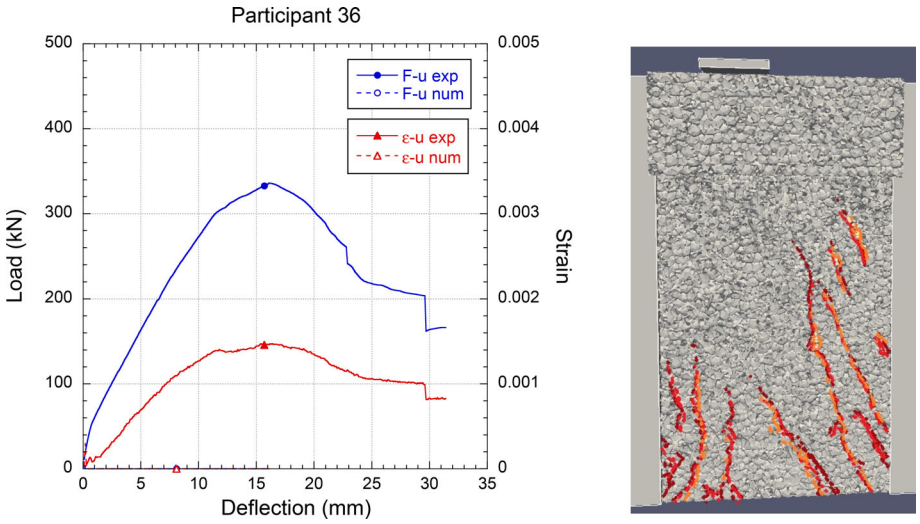


FIGURE A10 Results of participant 36

College of Civil and Transportation Engineering, Hohai University.

Tiago Valente,[1] Inês Costa,[1] Lúcio Lourenço,[1] Christoph de Sousa,[1] Felipe Melo,[1] Cristina Frazão[11]: CiviTest-Pesquisa de Novos Materiais para a Engenharia Civil, Lda., Vila Nova de Famalicão, Portugal.

Zhongyue Tracy Zhang,[1] Frank J. Vecchio[11]: University of Toronto, Canada.

Ziyang Zhang,[1] Linyou Zhang,[1] Weiting Chen,[1] Yong Li[11]: Department of Bridge Engineering, Southwest Jiaotong University, Chengdu, China.